Università degli Studi di Modena e Reggio Emilia

Dipartimento di Scienze della Vita

In vitro monitoring of cellular respiration of different tumor cell lines and the effect of drugs and metabolites.

Tesi sperimentale di Laurea Magistrale Chimica e Tecnologie Farmaceutiche (D.M. 270/04*) di:*

Claudio Gaffuri

Relatori:

Prof.ssa Gamberini Maria Cristina

Prof. Byrne Hugh J.

Anno Accademico 2024/2025

SUMMARY

ABSTRACT I

LIST OF ABBREVIATIONS II

1.INTRODUCTION 9

1.1 Cancer cells 9

1.1.1 Definition of cancer cell 9

1.1.2 Differences between cancer and normal cell 10

1.2 Cellular respiration 12

1.3 Glycolysis 13

1.3.1 Steps of the Glycolytic regulation and differences with cancer cells 14

1.4 Krebs cycle 17

1.4.1 The effects of glutamine in the metabolism of the cells 18

1.5 Oxidative phosphorylation 20

1.6 Warburg effect 22

1.7 Compounds used in the experiments 25

1.7.1 2-DG 25

1.7.2 Oligomycin 25

1.7.3 FCCP 26

2 AIM OF WORK 28

3 MATERIALS AND METHODS 29

3.1 Cells culture 29

3.1.1 Cell lines 29

3.1.2 Sterilization of biological safety cabinet and some safety procedures 29
3.1.3 Cultivation process 29
3.1.4 Counting cell process 31
3.1.5 Seeding cells into 96-well plate 33
3.1.6 Freezing and resuscitation procedure 33
3.2 Oxygen consumption assay 35
3.2.1 Description 35
3.2.2 Signal Optimization procedure 35
3.2.3 Planting cell 36
3.3 Conduct of the experiments 37
3.3.1 Measurement Parameters 37
3.3.2 General considerations 37
3.4 Experiments 40
3.4.1 Experiment 1 40
3.4.2 Experiment 2 42
3.4.3 Experiment 3 43
3.4.4 Experiment 4 46
3.4.5 Experiment 5 47
3.5 Data Acquisition and Analysis 50
4 RESULTS AND DISCUSSION 52
4.1 Experiment 1 52
4.2 Experiment 2 57
4.3 Experiment 3 62

4.4 Experiment 4 64
4.5 Experiment 5 66
4.6 Mathematical model in Mathlab 71
4.6.1 Structure of the model 73
4.6.2 Results of the model 77
5 CONCLUSIONS 81
6 BIBLIOGRAPHY 82

ABSTRACT

Studying tumor metabolism and how cells exploit the resources around them could provide important clues regarding the therapy which can be used to counteract it, directing the choice toward one drug rather than another or one procedure rather than another. This thesis investigates how mitochondrial metabolism, particularly O_2 consumption, can modify cell growth and development. O_2 utilization is controlled as far as possible by the utilization of substances such as Oligomycin and 2-DG, the increase or decrease of Glucose, Glutamine and Lactic Acid. Oxygen consumption is measured through a commercial assay based on a fluorescent sensor that reveals the O_2 concentration inversely within previously cultured tumor cell plates. Another fundamental step that would increase awareness in therapy could be predicting what is happening in the cell, always at the metabolic level, and for this reason the creation of a mathematical model can be an important support for this purpose. The model construction in this thesis is addressed with Matlab, a fundamental software for translating the language of metabolism into statistical, predictive, and interpretable mathematical language so that it can be applied and adapted. The construction of the model follows the main steps of cellular metabolism in a simplified way, not only in order to be able to adapt it to all cell types, even those different from those used in this thesis, but also because a more complex model including the enzymatic equilibrium constants would have required more time and instrumentation than those available for this project. The versatility was exploited as as a strength for possible use for other cells. The in vitro study of metabolism and model building could be a valuable combination in the fight against tumor.

LIST OF ABBREVIATIONS

2-DG	2-Deoxy-D-glucose
2-DG-6-P	2-deoxy-D-glucose-6-phosphate
AAC	Adenine nucleotide carrier
a-KG	a-ketoglutarate
a-KGDH	Alpha-ketoglutarate dehydrogenase
ALA	Alanine transaminase
ASP	Aspartate
B	Blank control
CF-	Cell free negative control
DMEM	Dulbecco's Modified Eagle Medium (1X) +Glutamax-I (low glucose)
DMSO	Dimethyl sulfoxide
ECAR	Extracellular acidification rate
ETC	Electron Transport Chain
F16BP	Fructose-1,6bisphosphate
F26BP	Fructose-2,6-bisphosphate
FADH2	Flavin adenine dinucleotide
FCCP	Carbonyl cyanide 4-(trifluoromethoxy)phenylhydrazone
FH	Fumarate hydratase
GLS	Glutaminase
GOT	Glutamate oxaloacetate transaminase
GPT	Glutamate pyruvate transaminase
HIF1	Hypoxia-inducible factor 1
IDH	Isocitrate dehydrogenase

IMM	Inner mitochondrial membrane
MxP	MitoXpress Xtra
NADH	Nicotinamide adenine dinucleotide
O	Oligomycin
OCR	Oxygen consumption rate
OXPHOS	Oxidative phosphorylation
PBS	Phosphate buffered saline
PDH	Pyruvate dehydrogenase complex
PDHK	Pyruvate dehydrogenase kinase
PEP	Phosphoenolpyruvate
PFK	Phosphofructokinase
PFKFB	Phosphofructokinase/fructose-2,6-bisphosphatase
PK	Pyruvate kinase
ROS	Reactive Oxygen Species
SDH	Succinate dehydrogenase
TCA	Tricarboxylic Acid cycle
TIGAR	TP53induced glycolysis and apoptosis regulator
TR-F	Time-resolved fluorescence instrument
UCP1	Uncoupling protein 1

1 INTRODUCTION

1.1 Cancer cells

1.1.1 Definition of cancer cell

Cancer cells are biological cells that have acquired abnormal, uncontrolled proliferative capacity and can contribute to the formation of a neoplasm (tumor). This proliferation damages healthy tissues and can cause a diverse array of disorders, each identified by the cell or tissue type of origin. An estimated statistic that one in every four individuals over the age of 65 will have battled cancer by 2040[1]. This multifaceted disease evolves through numerous steps, many malignant pathways leading to diverse tumor types and subtypes. Each pathway includes unique aberrations and consequentially acquired traits necessary for overcoming tissue-specific barriers in specific tumorigenesis pathways. Cancer cell plasticity, however, represents a critical layer of this complexity. This phenomenon allows cancer cells to adapt and change, making them even more resilient and difficult to treat. Understanding this plasticity is crucial for developing more effective therapeutic strategies, in fact the cellular plasticity empowers tumor cells to modify their phenotypes, facilitating their evasion from terminal differentiation. This characteristic significantly slows effective cancer management by reinforcing tumor response modification and inducing therapy resistance to the immune system[1]. There is the possibility that the cell's microenvironment such as hypoxia-induced methylation changes, impacts non-mutational epigenetic reprogramming, presenting a parallel path to cancer development, aside from genetic mutations, reflecting the intricate interplay between various factors influencing cancer progression. Cellular differentiation stages in healthy cells and tissues are dynamically controlled by activating or inactivating certain transcriptional factors. Because both variables contribute to the abnormal activation of developmental programs, the factors that encourage cellular plasticity during development and wound healing also produce phenotypic plasticity in cancer[2]. Tumor cells can change their phenotypes, becoming either more or less differentiated or more or less invasive/proliferative depending on the cell it came from, considering its origin and its possibility to differentiate.[1]

1.1.2 Differences between cancer and normal cell

There are some important characteristics that can be discussed that highlight the differences between a normal cell and a cancer cell. There are a lot of tumor types and an increasing plethora of subtypes includes various aberrations (and hence acquired capabilities and characteristics) that are the result of tissue-specific barriers necessarily bypassed during particular tumorigenesis pathways[1]. The designation of these hallmarks is based on parameters found to be universally relevant across the spectrum of human cancers. The eight hallmarks currently include the acquired ability for sustaining proliferative signaling, evading growth suppressors, resisting cell death, enabling replicative immortality, inducing/accessing vasculature, activating invasion and metastasis, reprogramming cellular metabolism, and avoiding immune destruction[2].

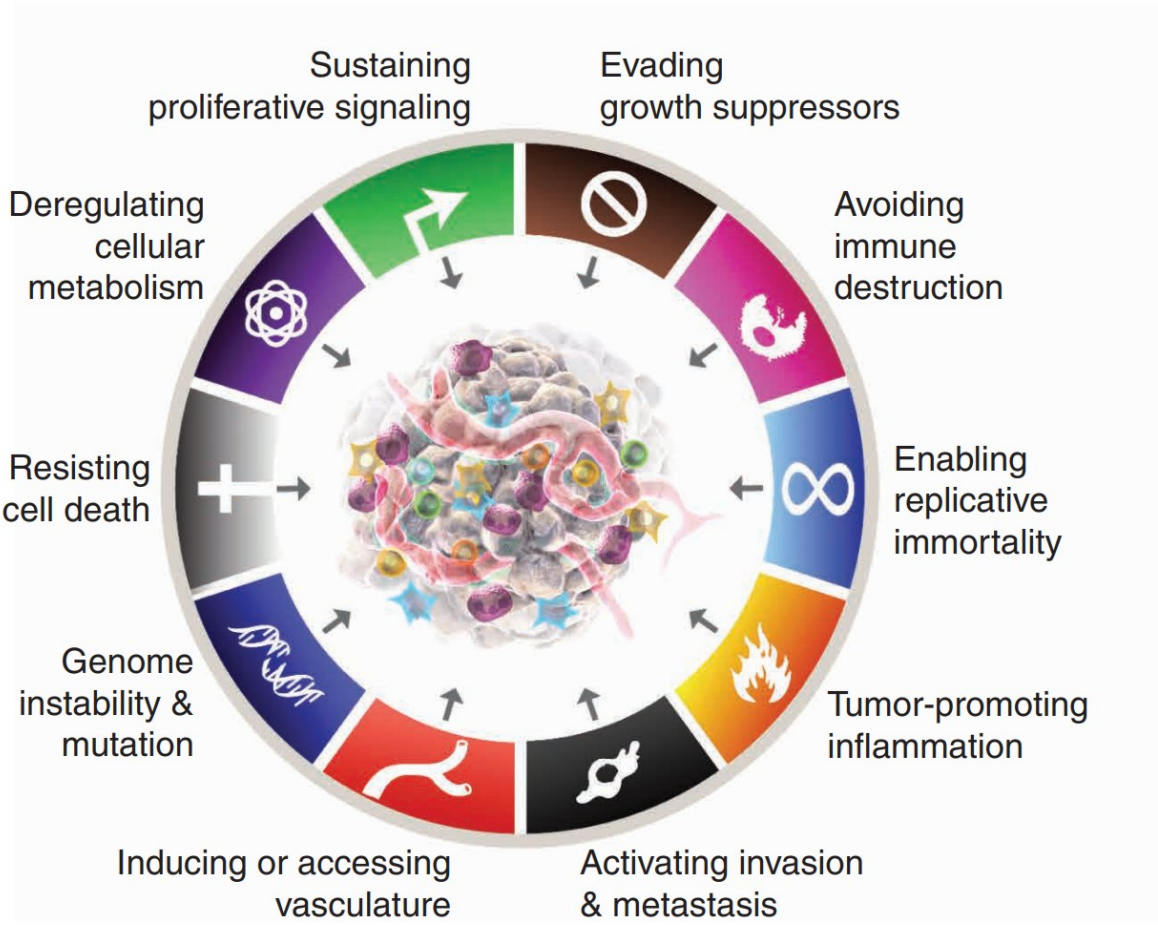

Figure 1 Schematic representation of the differences between a normal cell and a cancer cell. Based on Figure 1 in Hanahan, D. Hallmarks of Cancer: New Dimensions. Cancer Discovery ***2022.***

These hallmark traits in Figure 1 are the functional aberrant phenotypic capabilities that define

a mature tumor. However, these traits alone do not explain the process of how a normal cell evolves into a malignant one. Defining the enabling characteristics is important to underline which mechanisms lead a normal cell to become a tumor cell, these could define the driver of its evolution. These two enabling processes were genome instability and tumor-promoting inflammation. [2]

1.2 Cellular respiration

The main pathways to produce energy are glycolysis, TCA and oxidative phosphorylation. Under anaerobic conditions glucose is metabolized via glycolysis to generate pyruvate, which is converted into lactate, while, under aerobic conditions, pyruvate enters mitochondria for oxidative phosphorylation to produce more energy[3].

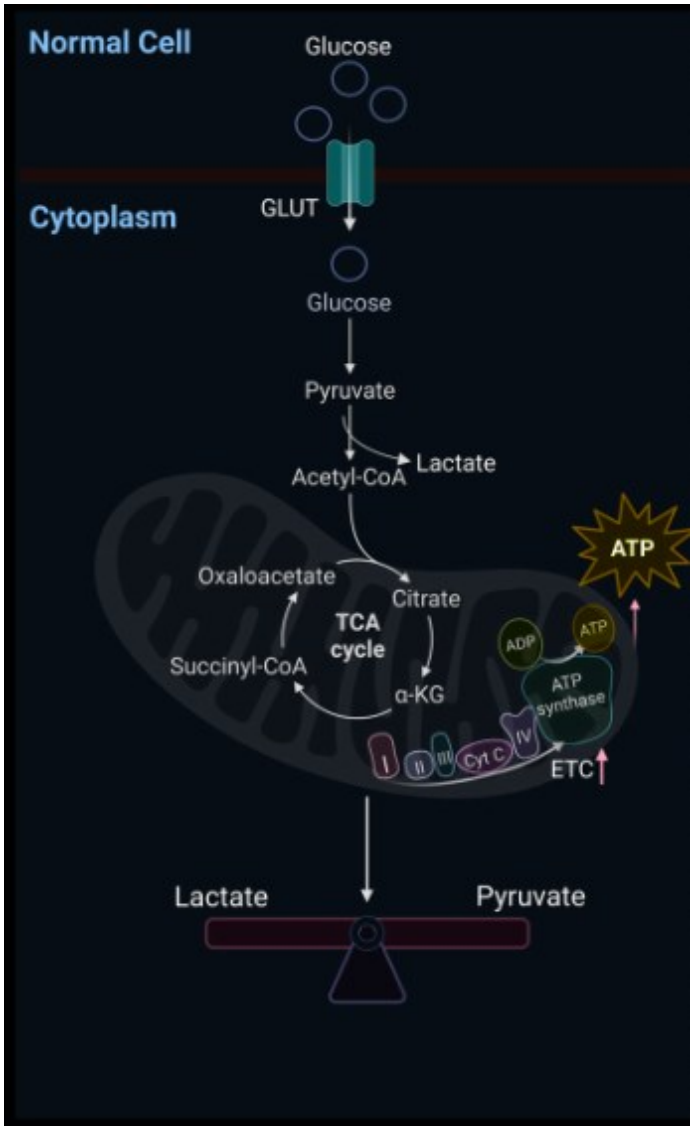

Figure 2 Schematic diagram of the cellular respiration with balancing of lactate and pyruvate production based on oxygen concentration in the cell. Based on figure 1 in Ma, F.; Yu, W. The Roles of Lactate and Lactylation in Diseases Related to Mitochondrial Dysfunction.

In Figure 2 there is a simplified pathway of glucose until the oxidative phosphorylation. There is even the deviation that leads to lactate, so we can have an overview of cellular respiration.

1.3 Glycolysis

Glycolysis is a 10-step metabolic pathway, which results in the production of pyruvate and two molecules of ATP. Concisely, upon entering the cell, glucose is phosphorylated to glucose-6-phosphate (G6P) by the enzyme hexokinase 2 (HK2) in the first and rate-limiting reaction of glycolysis[4]. Glucose-6-phosphate can enter the glycolytic or pentose phosphate pathway. Next, the enzyme glucose-6-phosphate isomerase catalyses the conversion of G6P to fructose-6-phosphate (F6P), which is converted to fructose-1,6-bisphosphate by the enzyme phosphofructokinase-1 (PFK-1) that uses ATP as the energy source. In the last step of glycolysis, ATP and pyruvate are produced by the enzyme pyruvate kinase, which catalyzes the irreversible transfer of the phosphoryl group from phosphoenolpyruvate to ADP. Overall, the net products of glycolysis are two molecules of ATP, two molecules of nicotinamide adenine dinucleotide (NADH), and pyruvate. In general, healthy cells rely on OXPHOS and glycolysis for ATP production; however, the energy contribution differs depending on the cell type and cellular microenvironment[4,5].

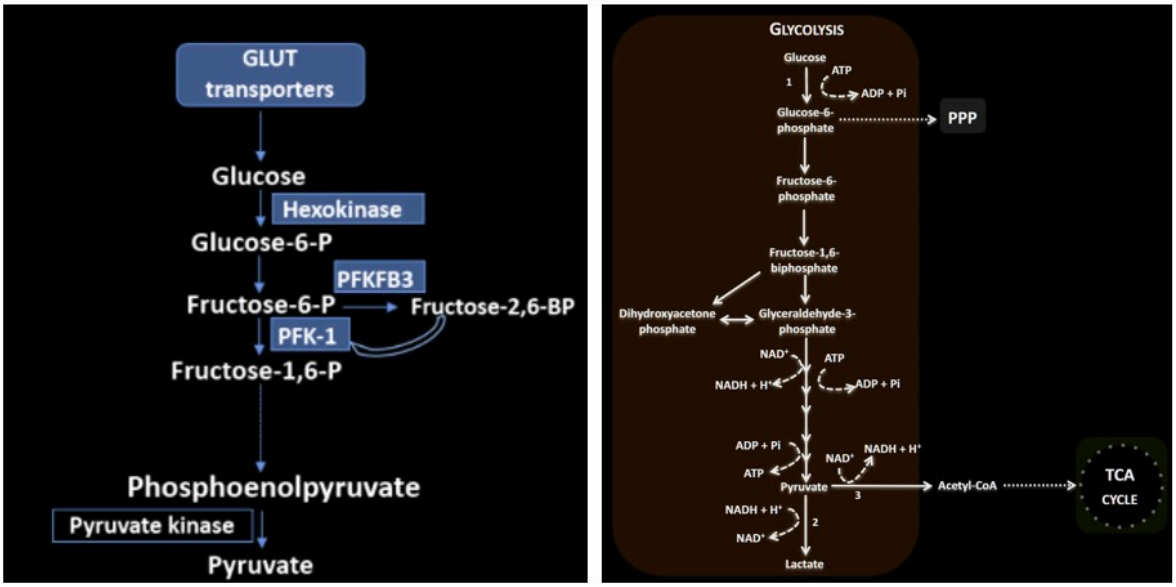

Figure 3 ***Schematic overview of the glycolytic pathway,*** *(Left) Simplified representation of the upper glycolytic steps, from glucose uptake via GLUT transporters through hexokinase-mediated phosphorylation to pyruvate production via pyruvate kinase, highlighting the regulatory roles of PFK-1 and PFKB3. Based on Figure 1 in Zlacká, J.; Zeman, M. Glycolysis under Circadian Control. IJMS 2021. (Right) Detailed representation of the complete glycolytic pathway, from glucose to pyruvate, including the branching points towards the pentose phosphate pathway (PPP), lactate production, and acetyl-CoA entry into the TCA cycle. Adapted from Fig. 1.1 in Mesquita, I.; Rodrigues, F. Cellular Metabolism at a Glance. In Metabolic Interaction in Infection.*

Under a normal condition of sufficient oxygen, 70% of ATP is produced in OXPHOS.

Conversely, in a hypoxic condition, the OXPHOS is weakened; therefore, the process of glycolysis is enhanced. The balance between OXPHOS and glycolysis helps to maintain cellular energy homeostasis. Aerobic glycolysis is considered a dominant metabolic pathway in activated endothelial, immune, and cancer cells. Most of the glucose is also converted to lactate when oxygen is available (Warburg effect)[6]. During the aerobic form of glycolysis, approximately four molecules of ATP are produced per glucose molecule. Even though aerobic glycolysis provides a lower ATP yield per glucose molecule compared to OXPHOS, it remains the preferred metabolic route when glucose is non-limiting, likely due to the faster rate of ATP production and the supply of carbon precursors[5]. If oxygen is available, enzyme pyruvate dehydrogenase (PDH) converts pyruvate to acetyl-Co-A, which enters the Krebs cycle in the mitochondria[4]. Acetyl-Co-A is then oxidized to carbon dioxide in cellular respiration. In the absence of oxygen, pyruvate is converted to lactate in a process known as anaerobic glycolysis. This conversion is catalyzed by lactate dehydrogenase (LDH) coupled with NADH to NAD+ oxidation. In anaerobic glycolysis, two molecules of ATP are produced from one molecule of glucose.[5]

1.3.1 Steps of the Glycolytic regulation and differences with cancer cells

Given the general background of glycolytic regulation, this section provides an overview of the broader context in which metabolic reprogramming supports cancer development and growth. Regulation occurs at multiple levels; one such level involves allosteric feedback and feed-forward mechanisms exerted by intermediate metabolites on their respective enzymes. Pivotal roles are played by three enzymes, phosphofructokinase (PFK), pyruvate kinase (PK) and phosphor - fructokinase/fructose-2,6-bisphosphatase (PFKFB) through their inhibition or activation by three reaction intermediates: fructose-1,6bisphosphate (F16BP), fructose-2,6-bisphosphate (F26BP) and phosphoenolpyruvate (PEP) in glycolysis. PFKFB is a bifunctional enzyme whose kinase and bisphosphatase domains catalyze the formation and hydrolysis reaction of F26BP, respectively. These enzymes have multiple isoforms (PFKL/M/P, PKM1/M2/L/R and PFKFB1-4) which are subjected to contrasting allosteric regulations this condition can affect the glycolytic activity in some different ways. By expressing distinct combinations of enzymatic isoforms, different cell types can achieve specialized glycolytic behavior[5,7]. This adaptation is crucial for aligning metabolic activity with the cell's unique energetic and biosynthetic priorities and growth necessity. In tumor formation caused by mutations in proto-oncogenes and tumor suppressors the loss of growth control is followed by alteration in the expression of specific glycolytic isozymes leading to

metabolic reprogramming. For example, HK2 is expressed at high levels in cancer cells, but it is only expressed in limited number of adult normal tissues. The inhibition of the release of cytochrome C to suppress apoptosis and promotes cell survival in cancer cells is promoted precisely by HK2, associates to outer mitochondrial membrane. Another example is PKM2, this is the typical isoform found in tumors, replacing it with PKM1 can reverse the cancer cell's metabolic profile. In experiments with H1299 lung cancer cells, swapping these isoforms caused a clear shift: the cells consumed less glucose and increased their mitochondrial respiration (OXPHOS), showing just how central PKM2 is to the tumor phenotype[7]. An additional layer of flux regulation of glycolysis is exerted by signaling pathways. Glycolytic flux is also regulated by signaling pathways, which can adjust the speed of the process without needing to switch enzyme isoforms. Instead, these pathways modify the kinetic properties of existing enzymes. For example, tyrosine kinase signaling can alter the activity of PKM2 by tuning its allosteric regulation, a key mechanism in how cancer cells manage their metabolism.

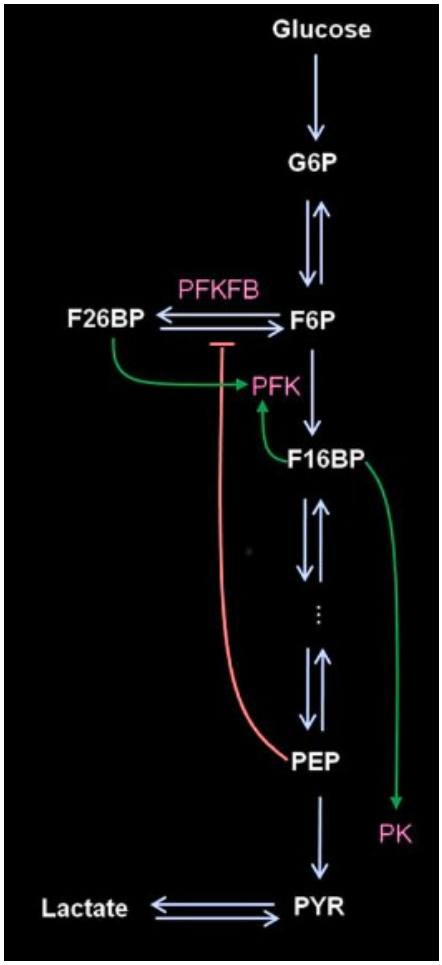

Figure 4 Representation of the key point of regulation of the Glycolysis. Figure 2 in Bistability in Glycolysis Pathway as a Physiological Switch in Energy Metabolism. PLoS ONE ***2014.***

In Figure 4 glycolysis exhibits a classical multiple steady state behavior in terms of its flux with respect to the glucose concentration, these are: high glycolytic flux states and low glycolytic flux states. Such bistable behavior is an output of complex allosteric regulations which in turn depend on the type of glycolytic isozymes expressed. This attitude will provide new insights on the regulation of cell metabolism improving the possibility to find new therapeutic perspectives.[7]

1.4 Krebs cycle

The TCA cycle is an aerobic pathway for the complete oxidation of several macromolecules, including glucose, fatty acids, and some amino acids[4]. Tricarboxylic acid (TCA) cycle is in the center of both catabolic and anabolic metabolism. TCA is a generally conserved metabolic pathway consisting of a cyclic series of chemical reactions that harness high-energy electrons from fuel sources, this energy will enter in the electron transport chain thank to some transports. The TCA cycle itself neither consumes molecular oxygen nor produces meaningful amounts of ATP; rather, the TCA cycle removes electrons (reducing equivalents) from inputs (e.g., acetyl-CoA), suppling key anabolic substrates and in maintaining energy production[8].

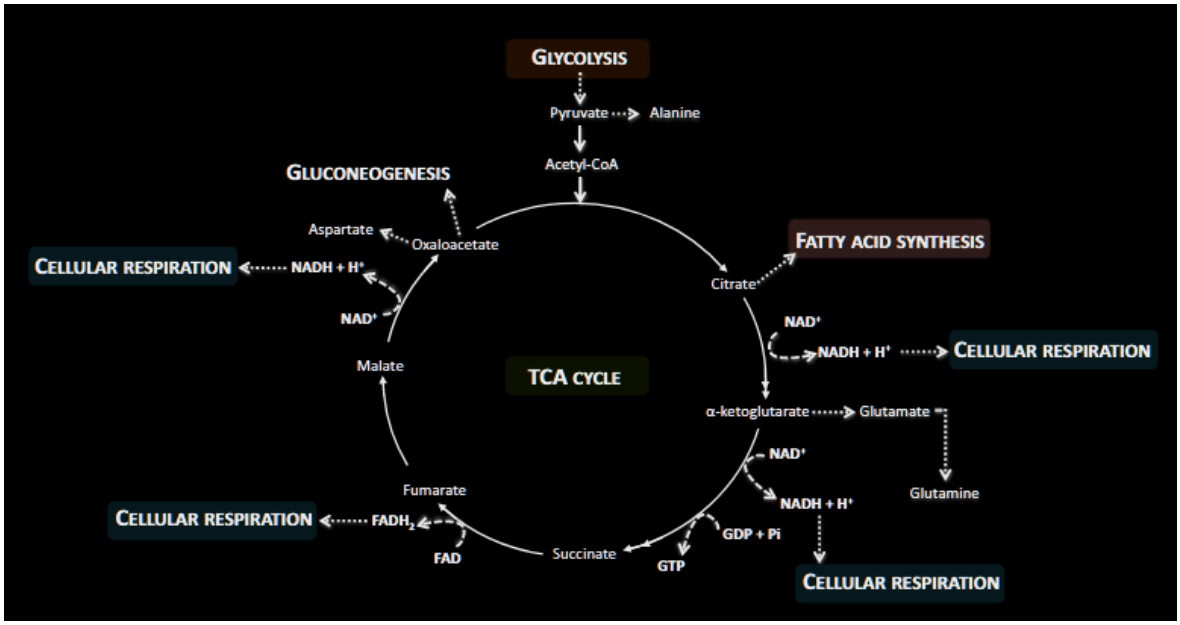

Figure 5 ***Schematic representation of the tricarboxylic acid (TCA) cycle and its metabolic connections*** *The TCA cycle operates as a central metabolic hub, linking glycolysis, gluconeogenesis, fatty acid synthesis, glutamine metabolism and cellular respiration through the sequential oxidation of acetyl-CoA and the generation of NADH and $FADH_2$. Figure 1.3 in Mesquita, I.; Rodrigues, F. Cellular Metabolism at a Glance.*

In Figure 5 there is the first step of the TCA cycle that is the condensation of acetyl-CoA with oxaloacetate by citrate synthase, which yields the six-carbon molecule citrate. The first primary control point in the TCA cycle occurs in the decarboxylation of isocitrate in α-ketoglutarate. NADH and ATP inhibit this reaction, in excess of pyruvate and acetyl-CoA citrate could accumulate and trigger lipid synthesis. The allosteric inhibition of α-ketoglutarate dehydrogenase, by succinyl-CoA and NADH, slowing its activity to convert

α-ketoglutarate into succinyl-CoA. Succinyl-CoA is further converted into succinate, with the production of GTP, and then the carbon skeleton is oxidized by succinate dehydrogenase (complex II of the ETC) to form fumarate, this will oxidize again to malate. This final intermediate is able to regenerate oxaloacetate, thus closing the cycle. Three molecules of NADH, one of FADH2, one of GTP, and two of CO_2 are the output of one cycle turn[4,8]. Each highly energetic reducing equivalent produced contains a pair of electrons that are substrates of the ETC. Pyruvate dehydrogenase complex (PDH) is a mitochondrial complex, this is responsible for the decarboxylation of pyruvate in acetyl-CoA engaging pyruvate carbons to be either converted into CO2 or shifted to de novo lipid synthesis, via export of mitochondrial citrate. Therefore, the PDH is highly regulated by both energy and redox state. Negative regulators of PDH activity are NADH, acetyl-CoA, and ATP in high concentration, this indicate high levels of energy and biosynthetic precursors, this situation activate the pyruvate dehydrogenase kinase (PDHK). PDHK regulates negatively PDH activity through phosphorylation. On the other hand, increased concentration of pyruvate signals availability of precursors for replenishment of the TCA cycle, consequently negatively modulating PDHK activity, increasing the flux through PDH. Therefore, cellular concentrations of acetyl-CoA, ATP, and NADH influence TCA cycle rate that is dependent from this substances, allowing a translation between biosynthesis and catabolism[4,8].

1.4.1 The effects of glutamine in the metabolism of the cells

In the realm of cellular metabolism, glycolysis and glutaminolysis serve as important pathways for energy production and biosynthesis of cellular building blocks. The glutaminolysis mechanism a-ketoglutarate (a-KG) derive from glutamine, which then goes through the tricarboxylic acid (TCA) cycle, refilling its intermediates and ultimately leading to the production of pyruvate and subsequently lactate. Recently, the glutaminolysis pathway has attracted attention for its key role in rapidly proliferating cells, serving as an alternative energy source to glycolysis in certain forms of cancer, a phenomenon known as “glutamine-addicted cancers”. Clearly, the presence of glutamine potentially influences the rate of the glycolytic pathway entering in the TCA cycle, maintaining redox balance, and supporting the biosynthesis of nucleotides, proteins and lipids, which in turn using more pyruvate into the mitochondria, this will process easily the pyruvate generated from glycolysis[8]. When glutamine enter into the mitochondria is initially deaminated to form glutamate in a reaction

catalysed by glutaminase (GLS), this will also produces NH4+, a metabolic by-product that triggers autophagy. In particular, the oncogene c-Myc has been shown to induce GLS expression, thereby enhancing glutamine catabolism to support cell survival and proliferation. There is a shift from glycolysis towards oxidative phosphorylation, due to the additional contribution of glutamine to energy production through the ETC (electron transport chain), reducing the glycolytic load[8,9]. Oligomycin, an ETC inhibitor, increases lactate production to the original glycolytic level, despite the presence of glutamine[9].

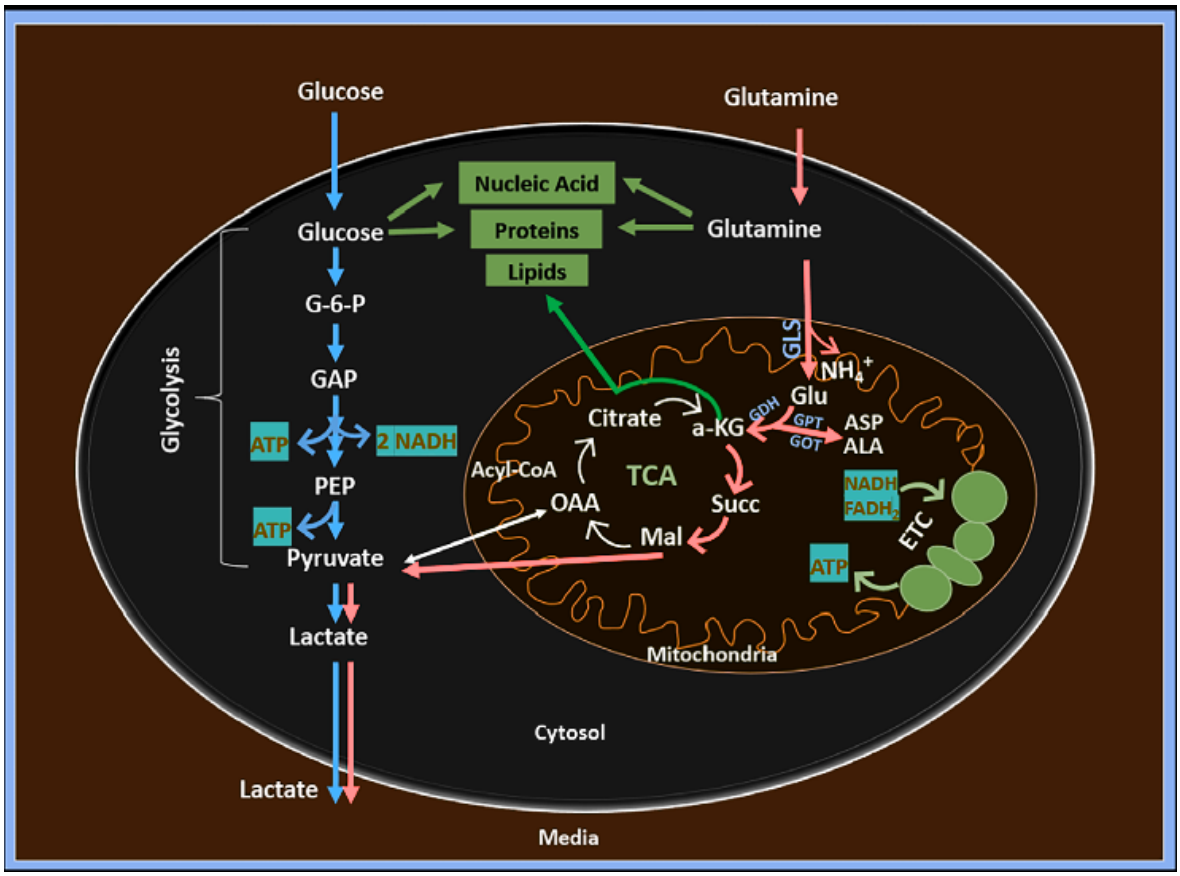

Figure 6 ***Overview of glucose and glutamine metabolism in a eukaryotic cell,*** *Schematic representation of the dual carbon substrate utilisation in tumour cell metabolism. Glucose (blue) fuels glycolysis and lactate production in the cytosol, while glutamine (pink) enters the mitochondria to feed the TCA cycle directly. Both substrates contribute to the biosynthesis of nucleic acids, proteins and lipids, as well as to ATP generation via the electron transport chain (ETC). Figure 2 in Mirveis, Z.; Patil, N.; Byrne, H. J. Experimental and Computational Investigation of the Kinetic Evolution of the Glutaminolysis Pathway and Its Interplay with the Glycolysis Pathway.*

In Figure 6 there is the evidence that the glutamine can enter in TCA cycle after its conversion in other amino acids such as aspartate (ASP) and alanine (ALA) enhanced by transaminases, including glutamate oxaloacetate transaminase (GOT) and glutamate pyruvate transaminase (GPT).

1.5 Oxidative phosphorylation

Oxidative phosphorylation is part of the cellular respiration, and it is its third stage after glycolysis and TCA. Oxidative phosphorylation (OXPHOS) happens in the mitochondria releasing adenosine triphosphate (ATP). OXPHOS is an enzymatic process defined as an electron transport linked reaction coupled to the ATP synthesis through an electrochemical transmembrane gradient promoted by a series of electron carriers embedded in the inner mitochondrial membrane. These are complex I (NADH ubiquinone oxidoreductase/NADH dehydrogenase), complex II (succinate ubiquinone oxidoreductase/succinate dehydrogenase), complex III (ubiquinol cytochrome c oxidoreductase/cytochrome bc1 complex), and complex IV (cytochrome c oxidase). OXPHOS is accomplished by complex V (ATP synthase). This process requires enough oxygen. Under the condition of oxygen deprivation, some of the normal cells can switch from OXPHOS to the glycolytic ATP production. The Tricarboxylic Acid (TCA) cycle and glycolysis produces nicotinamide adenine dinucleotide (NADH) and flavin adenine dinucleotide (FADH2) to store energy derived from the degradation of organic substances. These coenzymes carry the electrons necessary for OXPHOS to phosphorylating ADP to form ATP by the action of four protein complexes, which makes the electron transport chain (ETC). The complexes I and II receive electrons donated from FADH2 and NADH and shuttle electrons toward complexes III and IV, finally using oxygen molecules and releasing water the cell can obtain ATP. The shuffling of electrons through complexes I, III, and IV with the help of electron carriers produces the movement of protons [H^+] from the inner matrix of mitochondria to the intermembrane spaces, which produces a positive charge in the mitochondrial intermembrane space and negative charge in the matrix of mitochondria. This electrochemical difference mainly drives the production of ATP within the mitochondria.[10,11]

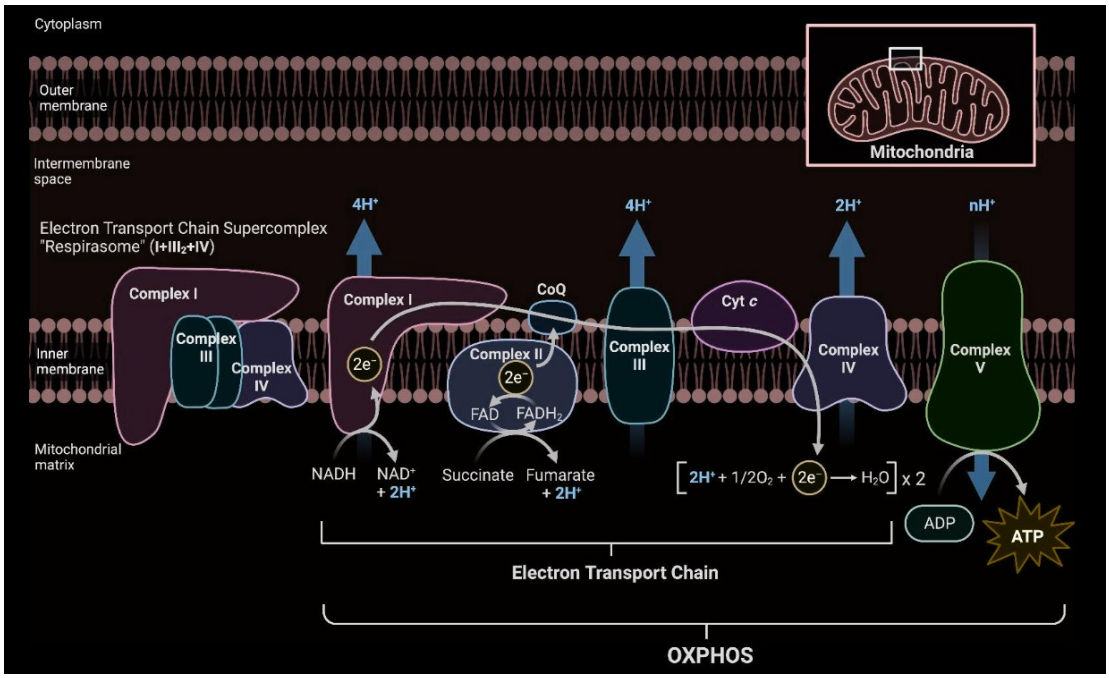

Figure 7 Representation of the five complex in the OXPHOS and the transport of electrons inside them. Figure 1 in Roles of Noncoding RNAs in Regulation of Mitochondrial Electron Transport Chain and Oxidative Phosphorylation. IJMS ***2023.***

In Figure 7 there is a zoom of the OXPHOS, this highlights the way of the electron so there is an evidence of the consumption of the oxygen. Some of these complexes generate higher-order assemblies called supercomplexes. In mammalian cells, a super complex called 'respirasome' is the major structure, which is composed of one complex I, two complex IIIs, and one complex IV (I + III2 + IV)[10]. During oxidative phosphorylation, 36 molecules of ATP are produced per glucose molecule[5].

1.6 Warburg effect

The Warburg effect describes how tumor metabolism works and it is considered a hallmark of cancer. These cells have accelerated conversion of glucose to lactate even in the presence of abundant oxygen. The presence of functional cytochromes proves that mitochondria in tumor cells are not defective. This suggests that the shift to glycolysis is a metabolic choice rather than a consequence of mitochondrial failure.[6,11] Active mitochondria are essential to encourage the growth of the tumor, mostly due to their biosynthetic activity which go beyond simply providing energy. Mitochondria, at several stages, satisfy the metabolic needs of cancer cells, significantly modify the synthesis of bioenergetics such as NADPH and ATP, and convert the various available nutrients into central building blocks which are required for the growth and functioning of the cells. Hitting mitochondria as a pharmaceutical target can open some ways to fight cancer in future therapy.[11] In these cancers, oxidative phosphorylation (OxPhos) continues normally, producing as much ATP as OxPhos in normal tissues under the same oxygen partial pressure.

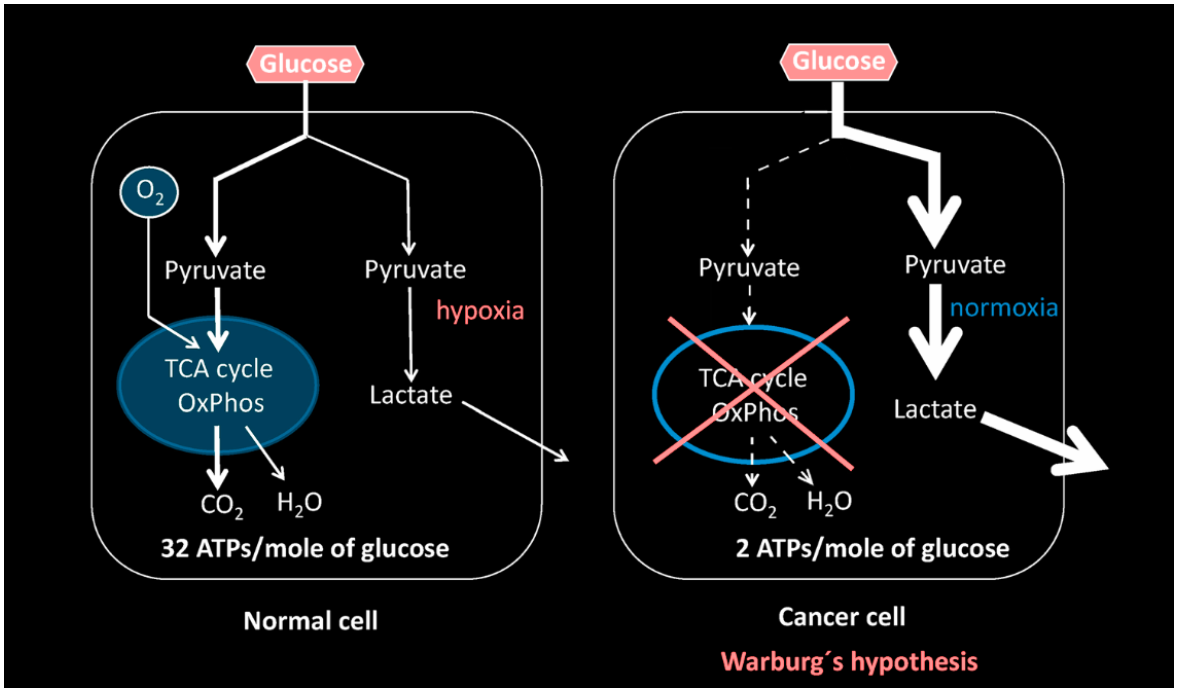

Figure 8 ***Schematic representation of the Warburg Effect,*** *In normal cells (left panel), glucose is metabolized to pyruvate, which under aerobic conditions enters the TCA cycle and oxidative phosphorylation (OxPhos), yielding up to 32 ATP per mole of glucose. Lactate production occurs only under hypoxic conditions. In cancer cells (right panel), pyruvate is preferentially converted to lactate even in the presence of oxygen (normoxia), bypassing mitochondrial metabolism entirely. This aerobic glycolysis produces only 2 ATP per mole of glucose, representing a markedly less efficient — yet metabolically advantageous — pathway that supports tumor growth and proliferation (Warburg's hypothesis). Figure 1 in Revisiting the Warburg effect: historical dogma versus current understanding*

While it is true that many cancer cells maintain functional mitochondria, recent evidence shows that specific damages can actually trigger the Warburg effect. Mutations in key TCA cycle enzymes such as fumarate hydratase (FH), succinate dehydrogenase (SDH), and isocitrate dehydrogenase (IDH) play a primary role in this process. These enzymatic defects, along with the altered activity of other mitochondria-linked proteins like pyruvate dehydrogenase (PDH) or alpha-ketoglutarate dehydrogenase (a-KGDH), lead to an abnormal accumulation of Reactive Oxygen Species (ROS). Far from being just toxic byproducts, these mitochondrial ROS function as powerful retrograde signals. They drive the entire oncogenic journey from the initial mutation to tumor proliferation and metastasis by forcing the cell to reprogram its metabolism and develop resistance to apoptosis[6,11]. Tumor cells express elevated levels of antioxidant proteins to prevent the accumulation of ROS pushing their self in the direction of a proliferative state by simultaneously resisting ROS-induced mitochondrial pore opening and subsequent cell death. Tumor cells can balance the generation of mitochondrial ROS allowing them to stay in their tumorigenic state with the desired levels of ROS. The production of mitochondrial ROS due to hypoxic conditions leads to the activation of hypoxia-inducible factor 1 (HIF1) this is very important because advances to metabolic swing from oxidative phosphorylation to glycolysis by enhancing the manifestation of glycolytic enzymes and expediting metastasis and tumorigenesis. The connection between mitochondrial ROS and HIF1 is complex as the over-synthesis of mitochondrial ROS activates HIF1, whereas the oxidative stress is alleviated upon activation of the glycolytic program in a reparation manner. In various forms of cancer, a decrease in the production of mitochondrial ROS by HIF1 promotes the growth of tumors and facilitates the existence of metastatic cells, hence, the targeting of mitochondrial ROS and antioxidants can be presented as a beneficial and novel therapy to manage cancer[11]. In healthy cells, tumor suppressor p53 regulates glucose metabolism by direct inhibition of glucose transporter expression. However, in cancer cells, insufficient p53 regulation contributes to an increased expression of cancer-associated glycolytic genes. Additionally, loss of p53 function can lead to increased glycolysis by downregulation of TIGAR (TP53induced glycolysis and apoptosis regulator). Under normal conditions, TIGAR slows down glycolysis by converting fructose-2,6-bisphosphate, an allosteric activator of PFK1 enzyme back to fructose-1-phosphate. It was confirmed that expression of glucose transporters, especially GLUT3, is controlled by NF-κB, whose activation can be

blocked by tumor suppressor p53. Therefore, reduced GLUT3 expression is followed by a decreased level of glycolysis. Mutation in p53 enhances the expression of GLUT3 mediated by NF-κB pathways, thereby facilitating glycolysis[5].

1.7 Compounds used in the experiments

1.7.1 2-DG

2-Deoxyglucose (2-DG) is a synthetic analogue of D-glucose where the hydroxyl group at the C-2 position is replaced by a hydrogen atom, allowing it to enter cells via GLUT1 and GLUT4 transporter crossing the blood-brain barrier. Once inside the cytoplasm, 2-DG is phosphorylated by hexokinase II to form 2-deoxy-D-glucose-6-phosphate (2-DG-6-P), which cannot be further metabolised due to the absence of the C-2 hydroxyl group required for the isomerisation step catalysed by phosphoglucose isomerase. The consequent intracellular accumulation of 2-DG-6-P apply competitive and allosteric inhibition of hexokinase, effectively blocking glycolytic flux and leading to a failure in ATP production and cell cycle arrest. This glycolytic blockade is particularly lethal in tumour cells under hypoxic conditions, where alternative ATP-generating pathways are unavailable, this causes a dramatic reduction of extracellular acidification rate and lactate production. Beyond its direct metabolic effects, 2-DG triggers a cascade of following signalling events[12]. The resulting drop in the intracellular ATP/AMP ratio activates AMP-activated protein kinase (AMPK), suppressing mTOR complex activity and inducing autophagy. While autophagy initially represents a pro-survival response, sustained autophagic flux finally drives the cell towards apoptosis. 2-DG further sensitises tumour cells to extrinsic apoptotic stimuli by downregulating anti-apoptotic proteins, and by inhibiting the pentose phosphate pathway reduces intracellular NADPH and glutathione levels, reducing antioxidant defences and promoting reactive oxygen species (ROS) accumulation. Notably, the ability of 2-DG to enhance autophagy represents a limiting factor for its autonomous anticancer efficacy, as it can temporally sustain cancer cell survival, making simultaneous targeting of multiple mitochondrial pathways a crucial consideration for its therapeutic application [11,12]. Autophagy is a cellular recycling mechanism that degrades internal components and damaged proteins to reclaim essential nutrients and energy, providing a temporary "life support" strategy for cells to survive metabolic or therapeutic stress[13].

1.7.2 Oligomycin

Oligomycin A is a macrolide antibiotic and potent inhibitor of the mitochondrial ATP synthase complex (F_0F_1-ATPase, Complex V of the respiratory chain). Its mechanism of

action relies on selective binding to the proton transport sites of the c-ring subunit within the transmembrane F_0 domain, thereby blocking the terminal step of oxidative phosphorylation and preventing ATP synthesis from ADP and inorganic phosphate. Since oxidative phosphorylation yields essentially more ATP per glucose molecule than glycolysis, its inhibition creates an acute energetic crisis that activates AMPK, this factor can control the energy usage of the cell[14,15]. AMPK-dependent reprogramming of cellular metabolism coordinately promotes glucose uptake, stimulates glycolytic flux, partly through activation of 6-phosphofructo-2-kinase, and suppresses anabolic ATP-consuming processes, collectively redirecting energy production towards glycolysis. This compensatory response is reflected experimentally in a marked increase in extracellular acidification rate (ECAR) due to enhanced lactate production. The amount of this glycolytic upregulation, however, depends on the baseline metabolic phenotype of the cell: in cells that already rely predominantly on anaerobic glycolysis, oligomycin-induced mitochondrial blockade produces little or no additional stimulation of glycolytic flux, as the pathway is already operating near saturation. Oligomycin's can target even human cell causing toxicity preventing its usage for human treatments. Nevertheless, structural and genetic studies have established that the oligomycin binding site defines a pharmacological target shared with other antibiotic classes, providing a valuable framework for the rational design of more selective therapeutic compounds.[14,15]

1.7.3 FCCP

Carbonyl cyanide 4-(trifluoromethoxy)phenylhydrazone (FCCP) is a mitochondrial uncoupling agent that has been studied widely in the context of cellular bioenergetics. It was long believed to work simply by shuttling protons across the inner mitochondrial membrane (IMM) through passive diffusion, bypassing ATP synthase. More recent studying, however, have challenged this view, showing that FCCP primarily acts by engaging specific membrane proteins, namely the adenine nucleotide carrier (AAC) in somatic tissues and uncoupling protein 1 (UCP1) in brown adipose tissue, rather than diffusing freely through the lipid bilayer[16,17]. These are the same proteins that mediate physiological thermogenesis in response to fatty acids. Studies suggest that FCCP fits into the translocation cavity of AAC when it faces the cytosol, where it facilitates proton entry into the mitochondrial

matrix. However, some degree of protein-independent proton transport remains, and this causes the off-target type effects observed at higher doses. In terms of metabolic consequences, FCCP collapses the proton gradient across the IMM, forcing the electron transport chain to improve its activity in a useless attempt to rebuild it. This drives oxygen consumption to its maximum while energy is dissipated as heat rather than captured as ATP. At low concentrations, this mild uncoupling can actually be beneficial, reducing mitochondrial ROS production in a way that approximate the action of natural uncoupling proteins[16,17]. At higher doses, though, the picture changes completely: instead of limiting ROS, FCCP amplifies their release and can trigger senescence, apoptosis, and in extreme cases severe cardiac dysfunction. This bell-shaped dose-response makes careful titration essential when using FCCP experimentally and is also the main reason why its potential therapeutic applications in metabolic diseases such as obesity and diabetes have not yet translated into clinical use[16,17].

2 AIM OF WORK

The main aim is to demonstrate the use of the commercial oxygen consumption assay to monitor the real-time metabolic responses of cells to feeding and metabolic modulation using drugs, and demonstrate how this can be augmented using a phenomenological kinetic rate equation model, thanks to a math basis build on Mathlab. In this project, parts of cellular respiration is monitored: oxidative phosphorylation, thanks to an assay that monitor the consumption of oxygen. Specifically, oxygen consumption is monitored using an assay that reads the concentration of a fluorophore giving a signal inversely proportional to O_2 concentration. A kinetic model is then constructed which allows prediction of the behavior of the metabolism of the cells based on what is introduced into the medium; concentration of Glucose, Glutamine and two drugs: 2-DG and Oligomycin to see how the cells used them and how the oxygen consumption changed. The predictions generated by the mathematical model can provide important insights into the metabolism of any cell type, given that all cells share the processes of cellular respiration, whether they are tumor cells or cells involved in diseases such as diabetes, atherosclerosis, or neurological disorders, where glucose consumption plays a fundamental role. It would also be possible to draw comparisons between mutated or diseased cells and healthy cells, studying the differences in order to identify the most effective pharmacological interventions.

3 MATERIALS AND METHODS

3.1 Cells culture

3.1.1 Cell lines

Three adherent cell lines were used: LLMCK2, HEPG2 and A549, as they were available in the laboratory.

- LLCMK2: Epithelial morphology that was isolated from the kidney of an adult monkey.

- A549: Lung tissue of a white, 58-year-old male with lung cancer.

- HEPG2: Human hepatoblastoma cell line.

3.1.2 Sterilization of biological safety cabinet and some safety procedures

1. Put on nitrile gloves and sterilize the hood with Virkon, then with 70% EtOH and wipe it dry. Virkon is a disinfectant with a wide virucidal, bactericidal and fungicidal activity spectrum. The effectiveness of Virkon is further enhanced by its excellent detergent properties, so that clean pathogen-free surfaces can be achieved.

2. Gather all other supplies needed – waste bottle (with ¼ filled Virkon solution), micropipettes, pipette tips, pipettor, pipette, T75/T25 flasks, centrifuge tubes.

3. Spray gloves and all supplies to put in the hood with 70% EtOH before they enter the hood. Place supplies back at least 4 inches from the front airflow. Work from left (clean) to right (used/contaminated/waste).

4. Turn on the UV light for 40-45 mins prior to work to kill all contaminants and to allow potential contaminated air to circulate out.

5. Clean up any spilled cells immediately.

6. Do not work over open cultures; this will allow contaminants to fall into the sterile cells or media.

7. When finished, make sure to clean the hood with Virkon, then with 70% EtOH and dry.

3.1.3 Cultivation process

Cells were cultured in Dulbecco's Modified Eagle Medium DMEM (1X) Glutamax-I (low

glucose), supplemented with 10% MSC-Qualified Fetal Bovine Serum (FBS), and 1% penicillin at 37°C in a 5% CO_2 incubator**.** FBS provides a wide variety of macromolecular proteins, low molecular weight nutrients, carrier proteins for water–insoluble components, and other compounds necessary for in vitro growth of cells, such as hormones and attachment factors. Serum also adds buffering capacity to the medium and binds or neutralizes toxic components.

Materials

- Complete growth medium
- PBS (autoclaved): Phosphate buffered saline is a non-toxic solution used in many biological laboratories. Unlike water, PBS prevents cells rupturing or shriveling up due to osmosis.
- Trypsin/trypsin-EDTA (dissociation reagent)
- Pipette (5, 10 or 25ml) and tips
- Pipettor
- Micropipette
- T25/T75 flask, plates or dishes
- Disposable, sterile tubes
- 37ºC incubator with humidified atmosphere of 5% CO_2

*PBS, trypsin and DMEM must be pre-warmed at 37ºC

Procedure

1. Put on nitrile gloves, sanitize with 70% EtOH.

2. Take out all pre-warmed materials from the water bath. Avoid making contact with the hot bath in the container caps, as this could be a possible source of contamination.

3. Check if cells are 70-80% confluent under microscope

4. If not confluent after 3 days, decant the media and replace it with fresh media. This will give the cells more nutrients to grow faster. Check again after 24h.

5. Check the media for any contamination – cloudiness, turbidity and clusters of white floating solids (indicating bacterial contamination). Turbid – discard and spray with Virkon overnight. If media turns orange, it means a lot of CO_2 presence. CO_2 is highly soluble in water to produce carbonic acid that ionizes H^+ and HCO_3^-. More CO_2 produces more H^+ ions and hence media turns to acidic pH.

6. If confluent, remove and discard cell culture media.

7. Wash with PBS (2x) – gently swirl to ensure washing of whole flask.

8. Add trypsin/trypsin-EDTA (0.25%) and gently swirl.

9. Incubate for 5 mins.

10. Observe cells under the microscope for detachment. If cells are less than 90% detached, increase the incubation time a few more minutes, checking for dissociation every 30 seconds.

11. When ≥ 90% of the cells have detached, tilt the vessel for a minimal length of time to allow the cells to drain. Add 1:1 or 1:2 volume of media to inactivate the trypsin and ensure to mix well to avoid cells clumping together. Note: Media will stop trypsin from digesting the cell. If cells are left too long in the trypsin solution, they will get digested and will lose viability.

12. Decant all cells and transfer them into a centrifuge tube (cell suspension). Set the centrifuge on 5 mins and 400G.

13. Remove the medium and the trypsin, the cell will remain attached to the bottom. Add new medium, take and release several times so that the cells detach from each other.

14. Use new flask and pipette cell suspension to flask and incubate.

3.1.4 Counting cell process

The Trypan Blue dye exclusion test is used to determine the number of viable cells present in a cell suspension[18]. It is based on the principle that live cells possess intact cell membranes that exclude certain dyes, such as trypan blue, Eosin, or propidium, whereas dead cells do not so a viable cell will have a clear cytoplasm whereas a non-viable cell will have a blue cytoplasm.

Materials

- Pipette
- Pipette tips
- Trypan blue (cell viability dye)
- Hemocytometer
- Cell counter
- Cover slip

- Eppendorf tube

Procedure

1. Spray hemocytometer and cover slip with 70% EtOH. Dry and fix the coverslip in position.

2. Take cell suspension (doing until passage number 13 of the procedure before) and mixed thoroughly. Ensure there aren't visible clumps.

3. Pipette 1:1 cell suspension and trypan blue in an Eppendorf tube and mix well.

4. Pipette 10µl of 1:1 cell suspension and trypan blue into the hemocytometer. Do not overfill.

5. Place the chamber in the microscope. Check for any visible clumps (if there are, mix cell suspension gently to break up clumps). If there are too many cells, dilute cell suspension with 1ml media.

6. Count the cells in the four corners of the hemocytometer as shown below. Count the clear cells and cells stained with blue (DEAD). Take the average (number of cells counted divided by 4).

Viable Cell Count = number of live cells/total cells * dilution factor

Non-viable Cell Count = number of dead cells/total cells * dilution factor

Percentage Viability = number of viable/total number of cells * 100.

CALCULATION

The hemocytometer is equilibrated to the number of 10^4 cells per ml.

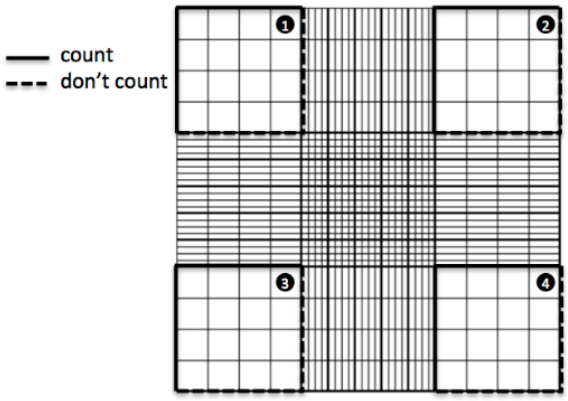

Figure 9 Illustration of hemocytometer

3.1.5 Seeding cells into 96-well plate

Materials

- Cell suspension
- DMEM
- 96-well plate (sterile)
- Micropipette
- Pipette tips (autoclaved)

Procedure

1. Take 96 well plate – label with name, experiment, date, incubation time.

2. Pipette a total volume of 200 µL with cells into each well, making at least 3 replicates.

3. Incubate cells for 24h to allow cells to adhere to the bottom of the wells. Don't rush to put plate in incubator; 30 min RT incubation beforehand can reduce edge effect.

4. Prepare the solution with components that you need so remove the used up medium and fill each well with 100 µL of solution.

5. Read the 96-plates.

3.1.6 Freezing and resuscitation procedure

To preserve cells, avoid senescence, reduce the risk of contamination, and minimize the

effects of genetic drift, cell lines may be frozen for long-term storage. Without the use of a cryoprotective agent, freezing would be lethal to the cells in most cases. Generally, cryoprotectant substance such as DMSO is used in conjunction with a complete medium for preserving cells at -70ºC or lower. DMSO acts to reduce the freezing point and allows a slow cooling rate. Gradual freezing reduces the risk of ice crystal formation and cell damage. DMSO is cell toxic when not frozen, so it is important to minimize the time the cells are exposed to liquid DMSO. Work quickly and maintain solutions cooled (especially for more sensitive cells).

Materials

- Freezing medium
- 90% complete DMEM
- 10% DMSO
- T25 flask labelled
- Water bath
- Pipette
- Pipettor

Protocol

1. Centrifuge desired number of cells ($1*10^5$ – $1*10^6$ cells/ml), re-suspend in medium, transfer to cryo vial with DMSO.

2. Place in a Styrofoam tube (or Mr. Frosty if available, which contains propanol for a constant freezing rate) which will allow gradual cooling rate and prevents damage to cells.

3. Place in -80ºC freezer overnight.

4. Take out cells from the freezer quickly into the water bath (do not wait for it to thaw at RT).

4. Cells should thaw approximately 1-2mins.

5. Quickly pipette thawed cells into T25 flask.

7. Add 5-7 ml of media and incubate overnight or 24h.

3.2 Oxygen consumption assay

3.2.1 Description

MitoXpress Xtra - Oxygen Consumption Assay (HS Method) is a highly flexible 96- or 384-well fluorescence plate reader-based approach, for the direct, real-time analysis of cellular respiration and mitochondrial function. The easy-to-use MitoXpress Xtra assay allows measurement of extracellular oxygen consumption rates (OCR) with whole cell populations (both adherent and suspension cells), isolated mitochondria, permeabilized cells and a wide range of 3D cultures including: tissues, small organisms, spheroids, scaffolds and matrixes. The assay is also suitable for measurement of isolated enzymes, bacteria, yeasts and molds. The MitoXpress Xtra reagent is chemically stable and inert, water-soluble and cell impermeable, making it the ideal and scalable mix-and-measure reagent for use in a wide range of cell culture conditions - all measured using a fluorescence plate-reader. In this assay, MitoXpress Xtra is quenched by O_2, through molecular collision, and thus the amount of fluorescence signal is inversely proportional to the amount of extracellular O_2 in the sample. Rates of oxygen consumption are calculated from the changes in fluorescence signal over time. The reaction is non-destructive and fully reversible (neither MitoXpress Xtra nor O_2 are consumed), facilitating measurement of time courses and drug treatments. HS Mineral oil must be put on top of each well needs to maintain the concentration of O_2 constant.

Before using MitoXpress Xtra you need to reconstitute that in a vial adding 1 mL of water, PBS or culture media, gently aspirating 3-4 times. Reconstituted probe stock can be stored in the dark between +2 to +8 °C for two days or stored as aliquots in water at -20 °C for use within one month (avoid freeze thaw).

3.2.2 Signal Optimization procedure

STEP 1: Prepare eight replicate wells of a 96-well plate by adding 90 µL prewarmed culture medium to each well (A1-A4, B1-B4).

STEP 2: Add 10 µL reconstituted MitoXpress Xtra reagent to four of the replicate wells (A1-A4) and 10 µL water, PBS or media to the remaining replicates wells (B1-B4).

STEP 3: Promptly add two drops (or 100 µL) prewarmed HS Mineral Oil to all eight replicate wells, taking care to avoid air bubbles.

STEP 4: Read plate immediately in a fluorescence plate reader for over 30 minutes (read every 2-3 minutes).

STEP 5: Examine Signal Control well (A1-A4) and Blank Control well (B1-B4) readings and calculate S:B ratio using the last reading at 30 minutes.

3.2.3 Planting cell

All constituents for planting cells must be pre-warmed at 37° C in an incubator even the 96-well plate.

STEP1: For Adherent cells, seed cells in a 96-well plate in 200 µL culture medium. Incubate overnight in a CO_2 incubator at 37 °C.

To assess Oxygen Consumption or to investigate the effect of a compound on electron transport chain function (ETC; oxidative phosphorylation), cells are treated immediately prior to measurement. To reduce time;

STEP 2: Remove spent culture medium from all assay wells and replace with 90 µL of fresh culture media.

STEP 3: Add 10 µL reconstituted MitoXpress reagent to each well, except those wells for use as Blank Controls. Add 10 µL of fresh culture media to these Blank Control wells.

STEP 4: Test compound stock or vehicle may be added at this point if desired.

STEP 5: Promptly seal each well by adding two drops (or 100 µL) prewarmed HS Mineral Oil, taking care to avoid air bubbles.

STEP 6: Read the plate immediately in a fluorescence plate reader. The plate should be measured kinetically for > 90 minutes.

3.3 Conduct of the experiments

3.3.1 Measurement Parameters

MitoXpress Xtra reagent is a chemically stable and inert, biopolymer-based, cell impermeable oxygen-sensing fluorophore[19].

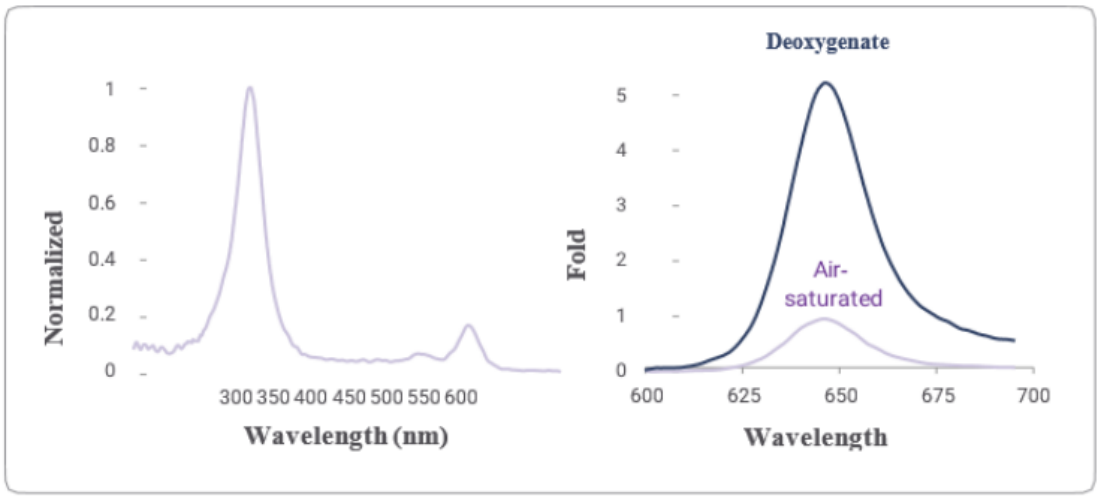

Figure 10 Excitation and Emission spectra of MitoXpress Xtra. Left panel shows normalized excitation (Ex 360-400 nm; Peak 380 nm). Right panel shows emission (Em 630 - 680 nm; Peak 650 nm) in oxygenated and deoxygenated conditions.

The instrument that I used was Time-resolved fluorescence (TR-F). TR-F measurement reduces nonspecific background and increases probe sensitivity. Optimal delay time is ~30 µs and gate (integration) time is 100 µs. TR-F has plate temperature control, that I set to 37° C. The numbers of flashes after optimization were 20 from 3. The reading mode of the instrument was set to be from the bottom, because on the top of the wells there was the oil that could refract the light decreasing the efficiency of the reading. The instrument had to be pre-warmed at 37°C using its temperature control, even during the experiment.

3.3.2 General considerations

For each experiment, a table was drawn to represent the 96-well plate to take note about the position of the solution and the cell lines as in Figure 11, in this way the data could be analyzed better and faster.

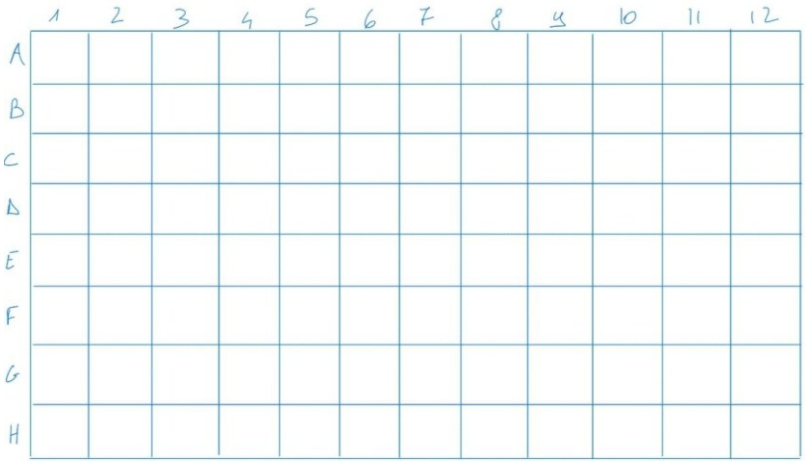

Figure 11 Representation of 96-well plate

For each experiment, after the calculations of the molarity of solutions' components, one Eppendorf per solution was prepared that had the total amount of components of one well multiplicated per three replicates of one well multiplicate again per the number of cell lines that I used in that experiment. Then, using a single pipette, the amount of the solution per one well in a 96-well plate without the cells was transferred, based on the table prepared earlier. In this way, a multiple pipette with eight tips could be used to take the solution per eight wells in one shot, releasing the solution per one well into eight wells more rapidly. Obviously, the tips were changed for every solution. The multiple pipette was used even to remove the consumed medium after 24 hours from the 96-well plate with cells taking care to not detach the cells from the bottom of the well.

All the components must be pre-warmed before their use including the 96-well plates, the HS oil and the solutions too, so the stage of the release of the solution into the wells needed to be fast. HS oil was used to cover every well, even the control, to avoid changing in oxygen concentration, thanks to a repeater pipette (provided by the manufacturer). Two or three drops of oil were used, avoiding the formation of air bubble keeping the repeater pipette inclined 45° (as suggested by the productor), after which the reading was started. For every experiment, three wells each were used as control, these were:

Blank control (B): Add in total 100 µL of fresh culture media. Do not add MitoXpress Xtra reagent to these wells.

Cell free negative control (CF-): Add 90 µL of fresh culture media + 10 µL of reconstituted

MitoXpress Xtra reagent to each well.

The cell density suggested by the manufacturer was 60000-80000 cell per well and even the quantity of MxP of 10µL.

The concentrations chosen for 2-DG, Oligomycin, Glucose ang Glutamine were taken from the experiment on the production of lactic acid done by Nitin Patil and Zohreh Mirveis, both PhDs that follow main project[9,20].

3.4 Experiments

3.4.1 Experiment 1

In this experiment, the cells were starved; after the 24h of the seeding the medium was removed, 100 µL of Glucose free respiration buffer was added and the cells were incubated in the incubator without CO_2, then the solution was added and the reading performed. Run time: 2h:09

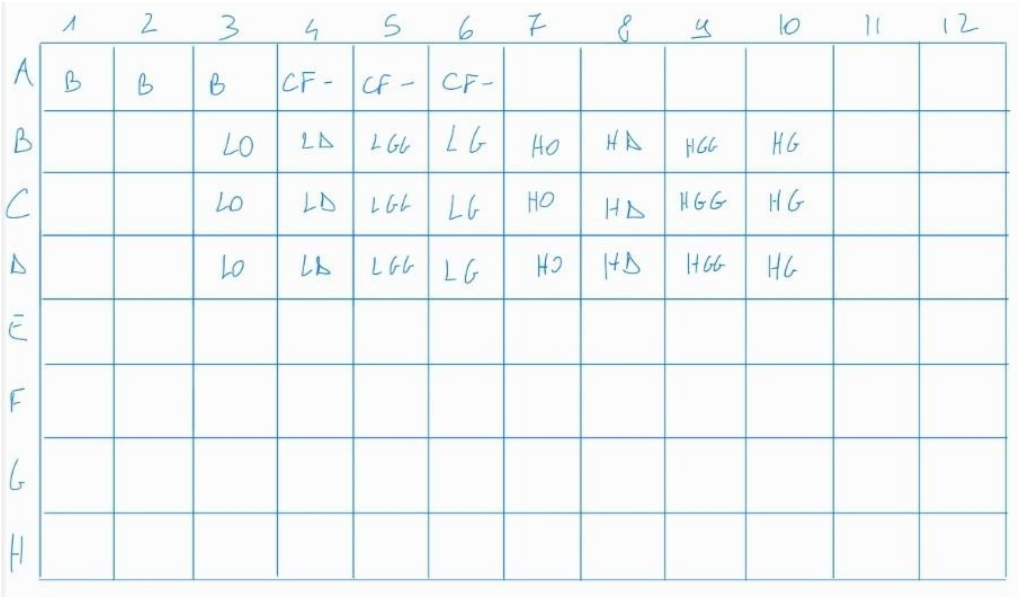

Figure 12 Representation of the table of the first experiment. L: LLMCK2, H: HEPG2, O: Oligomycin, D: 2-DG, G: glucose, GG: glucose plus glutamine, B: blank, CF-: control cells free.

In this experiment, the A549 line could not be used, due to their low density instead the other two lines were ready for the experiment.

Cell counting

LLMCK2: 173 (cells counted by the hemocytometer)/4 = $43*10^4$

430000cells : 1000 µL = 60000cells : X µL → X= (60000*1000)/430000 = 140 µL/mL

A549: 65/4 = $16*10^4$

X = 375 µL/mL, this result is too high to obtain the density needed.

HEPG2: 371/4 = $93*10^4$

X = 65 µL/mL

The calculated quantity per mL per each well was seeded. bringing volume to 200 µL with DMEM. The next calculations will be done on 100µL, the volume suggested by the assay manufacturer.

Preparation of the solutions

Concentrations used: 100mM 2-DG | 2 µM O | 20 mM Glucose | 2mM Glutamine

Cf * Vf = Ci * Vi

2-DG: 100mM * 0.1 mL = 500 mM * X mL

X= (100*0.1)/500 = 0.02mL

Oligomycin: 2µM * 100µL = 100 µM *X

X= 12µL

Glucose: 20mM * 0.1mL = 100mM * X

X= 0.02mL

Glutamin: 2mM * 0.1 µL = 10mM * X

X= 0.02mL

Preparation of the Eppendorf:

Total volume: 100µL

Eppendorf 1: (20µL 2-DG + 20µL Glucose + 10µL MxP + 50 µL DMEM) *3 (wells) *2 (cell lines)

Eppendorf 2: (2 µL O + 20µL Glucose + 10µL MxP + 68 µL DMEM) *3 (wells) *2 (cell lines)

Eppendorf 3: (20µL Glucose + 10µL MxP + 70 µL DMEM) *3 (wells) *2 (cell lines)

Eppendorf 4: (20 µL Glutamine + 20µL Glucose + 10µL MxP + 50 µL DMEM) *3 (wells) *2 (cell lines)

3.4.2 Experiment 2

Cells were not starved. Run time: 2h:09

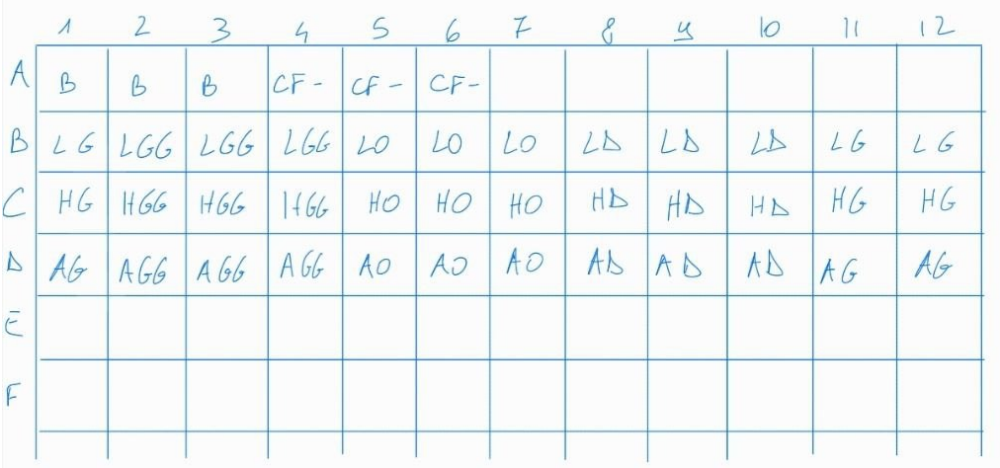

Figure 13 Representation of the table of the first experiment. L: LLMCK2, H: HEPG2, A: A549, O: Oligomycin, D: 2-DG, G: glucose, GG: glucose plus glutamine, B: blank, CF^-: control cells free.

Cell counting

LLMCK2: $578/4 = 144*10^4$

X= (60000*1000)/1440000 = 41 µL/mL

A549: $165/4 = 41*10^4$

X = 146 µL/mL

HEPG2: $248/4 = 62*10^4$

X = 97 µL/mL

Preparation of the solutions

Concentrations used: 100mM 2-DG | 2 µM O | 20 mM Glucose | 2mM Glutamine

Cf * Vf = Ci * Vi

2-DG: 100mM * 0.1 mL = 500 mM * X mL

X= (100*0.1)/500 = 0.02mL

Oligomycin: 2µM * 100µL = 100 µM *X

X= 12µL

Glucose: 20mM * 0.1mL = 100mM * X

X= 0.02mL

Glutamin: 2mM * 0.1 µL = 10mM * X

X= 0.02mL

Preparation of the Eppendorf:

Total volume: 100µL

Eppendorf 1: (20µL 2-DG + 20µL Glucose + 10µL MxP + 50 µL DMEM) *3 (wells) *2 (cell lines)

Eppendorf 2: (2 µL O + 20µL Glucose + 10µL MxP + 68 µL DMEM) *3 (wells) *2 (cell lines)

Eppendorf 3: (20µL Glucose + 10µL MxP + 70 µL DMEM) *3 (wells) *2 (cell lines)

Eppendorf 4: (20 µL Glutamine + 20µL Glucose + 10µL MxP + 50 µL DMEM) *3 (wells) *2 (cell lines)

3.4.3 Experiment 3

In this experiment, some modifications were introduced to improve the quality of the results: 80000 cell density, 15 µL of MxP, glucose respiration buffer was used as medium, 80 µL as total volume per each wells. Run time: 3h:17

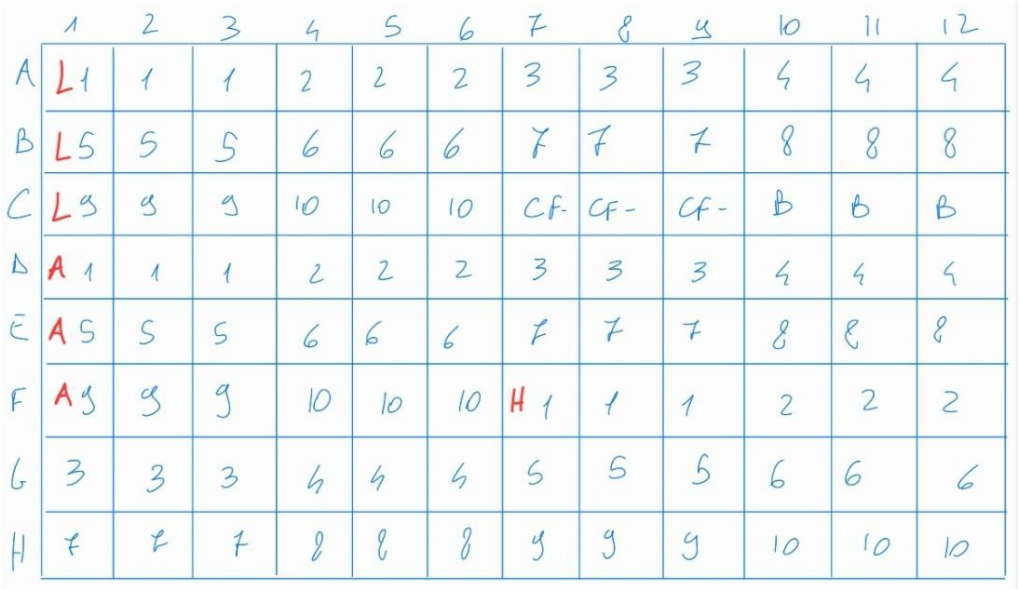

	1	2	3	4	5	6	7	8	9	10	11	12
A	L1	1	1	2	2	2	3	3	3	4	4	4
B	L5	5	5	6	6	6	7	7	7	8	8	8
C	L9	9	9	10	10	10	CF-	CF-	CF-	B	B	B
D	A1	1	1	2	2	2	3	3	3	4	4	4
E	A5	5	5	6	6	6	7	7	7	8	8	8
F	A9	9	9	10	10	10	H1	1	1	2	2	2
G	3	3	3	4	4	4	5	5	5	6	6	6
H	7	7	7	8	8	8	9	9	9	10	10	10

Figure 14 Representation of the table of the first experiment. L: LLMCK2, H: HEPG2, A: A549, B: blank, CF- : control cells free, 1-9 different solutions.

Cell counting

LLMCK2: $1684/4 = 421*10^4$

X= (80000*1000)/4210000 = 19 µL/mL

A549: $385/4 = 96*10^4$

X = 83 µL/mL

HEPG2: $472/4 = 118*10^4$

X = 67 µL/mL

Preparation of the solutions and Eppendorf

1: Glucose+Glutamine 20mM:1mM 2: (1) + 2 µM O

3: (1) + 100mM 2-DG

4: Glucose+Glutamine 20mM:10mM 5: (4) + 2 µM O

6: (4) + 100mM 2-DG

7: Glucose+Glutamine 20mM:20mM 8: (7) + 2 µM O

9: (7) + 100mM 2-DG

10: Glucose 20mM

1:	Glucose 20mM * 0.08mL = 100mM * X → X=16 µL	Medium: 41 µL
	Glutamine 1mM* 0.08mL = 10mM * X → X=8 µL	MxP: 15µL
2:	1+ Oligomycin 2 µL * 80 µL = 100 µL * X → X = 1.6 µL	Media: 39.4 µL MxP: 15 µL
3:	1+ 2-DG 100mM * 0.08 mL = 500 mM * X → X = 16 µL	Media: 25 µL MxP: 15 µL
4:	Glucose 20mM * 0.08mL = 100mM * X → X=16 µL	Medium: 9 µL
	Glutamine 10mM* 0.08mL = 20mM * X → X=40 µL	MxP: 15µL
5:	4+ Oligomycin 2 µL * 80 µL = 100 µL * X → X = 1.6 µL	Media: 7.4 µL MxP: 15 µL
6:	Glucose 20mM * 0.08mL = 100mM * X → X=16 µL	Media: 17 µL
	Glutamine 10mM* 0.08mL = 50mM * X → X=16 µL	MxP: 15 µL
	2-DG 100mM * 0.08 mL = 500 mM * X → X = 16 µL	
7:	Glucose 20mM * 0.08mL = 100mM * X → X=16 µL	Media: 17 µL
	Glutamine 20mM* 0.08mL = 50mM * X → X=32 µL	MxP: 15 µL
8:	7+ Oligomycin 2 µL * 80 µL = 100 µL * X → X = 1.6 µL	Media: 15.4 µL MxP: 15 µL
9:	7+2-DG 100mM * 0.08 mL = 500 mM * X → X = 16 µL	Media: 1 µL MxP: 15 µL
10:	Glucose 20mM * 0.08mL = 100mM * X → X=16 µL	Media: 49 µL MxP: 15 µL

3.4.4 Experiment 4

In this experiment it was used 80 µL as total volume per each wells. Run time: 2h:01:09, number of cycles: 300

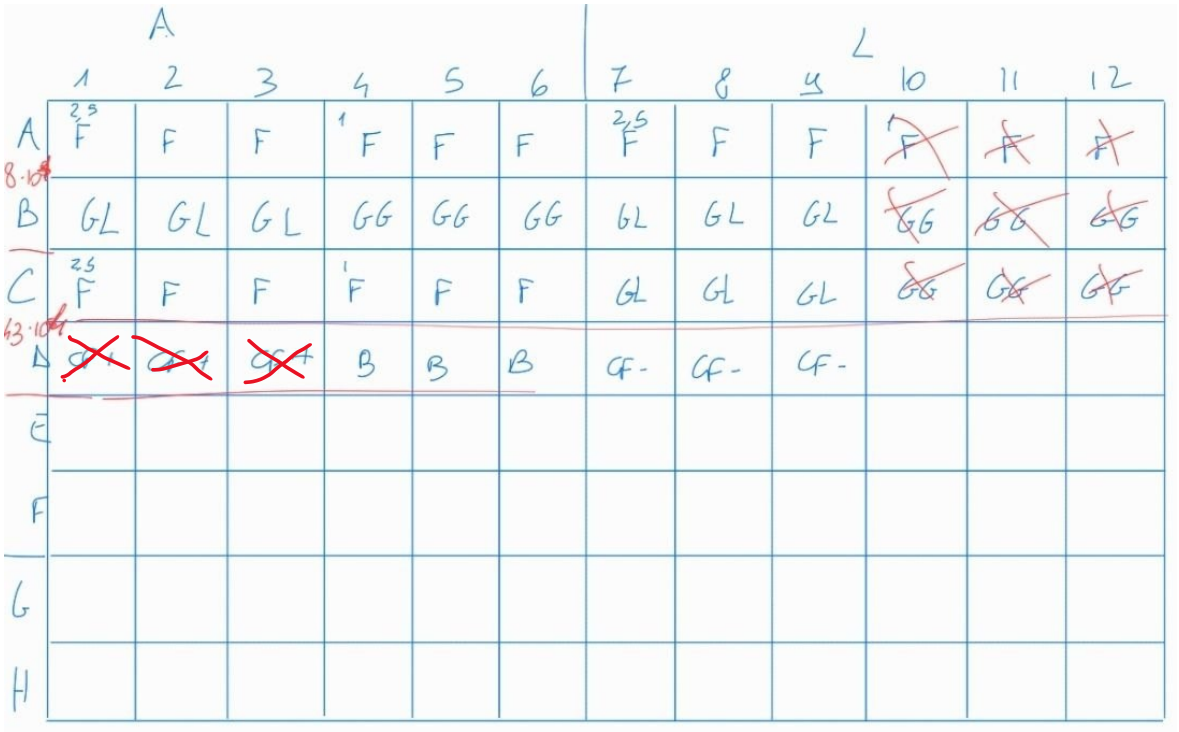

Figure 15 Representation of the table of the first experiment. L: LLMCK2, A: A549, O: Oligomycin, D: 2-DG, G: glucose, GG: glucose plus glutamine, B: blank, CF⁻: control cells free.

Cell counting

A549: $873/4 = 218*10^4$

2180000:1000µL = 80000:X X = 36 µL/mL Cells density for line A and B in Figure 15

2180000:1000µL = 430000:X X = 197 µL/mL Cells density for line C and D in Figure 15

Preparation of the solutions and Eppendorf

1: Glucose 20mM * 0.08mL = 100mM * X → X=16 µL Medium: 15 µL

Glutamine 20mM* 0.08mL = 50mM * X → X=32 µL MxP: 15µL

	FCCP 0.001 mM*0.08mL = 0.1mM * X → X=0.8 µL	
2:	Glucose 20mM * 0.08mL = 100mM * X → X=16 µL	Medium: 15 µL
	Glutamine 20mM* 0.08mL = 50mM * X → X=32 µL	MxP: 15µL
	FCCP 0.0025 mM*0.08mL = 0.1mM * X → X=2 µL	
3:	Glucose 20mM * 0.08mL = 100mM * X → X=16 µL	Medium: 49 µL
	Lactate 20mM* 0.08mL = 100mM * X → X=16 µL	MxP: 15µL
4:	Glucose 20mM * 0.08mL = 100mM * X → X=16 µL	Medium: 17 µL
	Glutamine 20mM* 0.08mL = 50mM * X → X=32 µL	MxP: 15µL

3.4.5 Experiment 5

In this experiment there is just A549 line. Run time: 2h:35, 250 cycles.

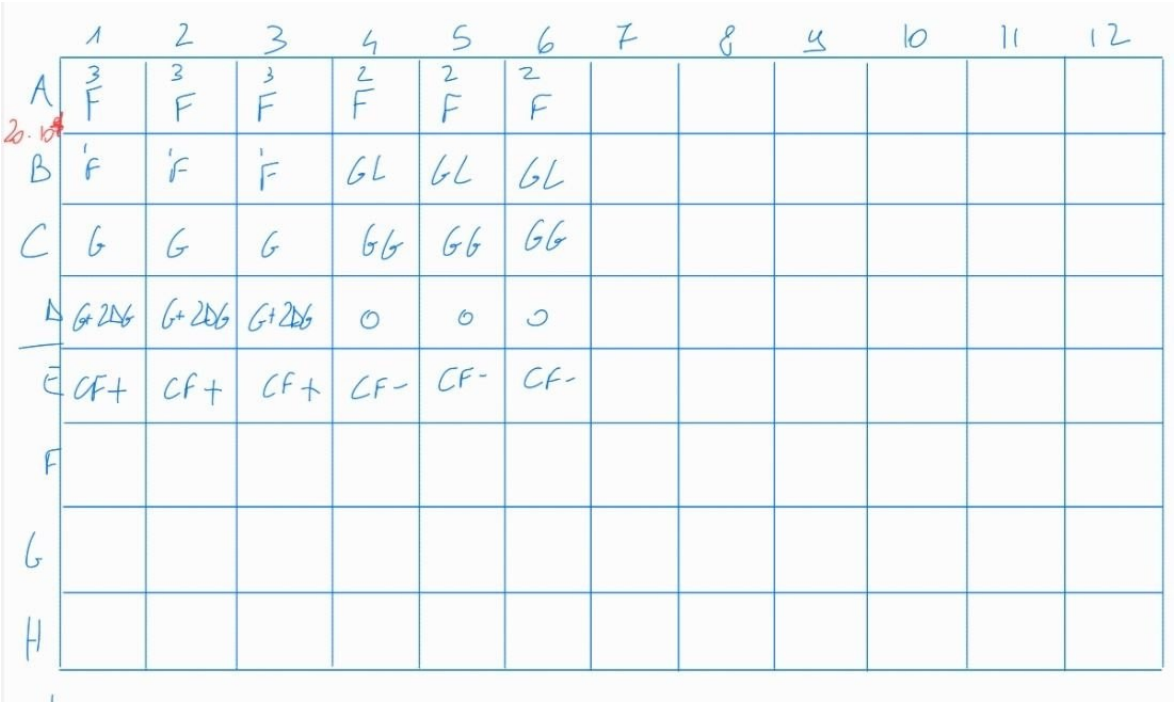

Figure 16 Representation of the table of the fifth experiment of the line A549, O: Oligomycin, D: 2-DG, G: glucose, GG: glucose plus glutamine, B: blank, CF-: control cells free.

Cell counting

A549: 1052/4 = $263*10^4$

2180000:1000µL = 250000:X X = 95 µL/mL

Preparation of the solutions and Eppendorf

1:	Glucose 20mM * 0.08mL = 100mM * X → X=16 µL	Medium: 15 µL
	Glutamine 20mM* 0.08mL = 50mM * X → X=32 µL	MxP: 15µL
	FCCP 0.003 mM*0.08mL = 0.1mM * X → X=2.4 µL	
2:	Glucose 20mM * 0.08mL = 100mM * X → X=16 µL	Medium: 15 µL
	Glutamine 20mM* 0.08mL = 50mM * X → X=32 µL	MxP: 15µL
	FCCP 0.002 mM*0.08mL = 0.1mM * X → X=1.6 µL	
3:	Glucose 20mM * 0.08mL = 100mM * X → X=16 µL	Medium: 15 µL
	Glutamine 20mM* 0.08mL = 50mM * X → X=32 µL	MxP: 15µL
	FCCP 0.001 mM*0.08mL = 0.1mM * X → X=0.8 µL	
4:	Glucose 20mM * 0.08mL = 100mM * X → X=16 µL	Medium: 33 µL
	Lactate 20mM* 0.08mL = 100mM * X → X=16 µL	MxP: 15µL
5:	Glucose 20mM * 0.08mL = 100mM * X → X=16 µL	Medium: 49 µL
		MxP: 15µL
6:	Glucose 20mM * 0.08mL = 100mM * X → X=16 µL	Medium: 17 µL
	Glutamine 20mM* 0.08mL = 50mM * X → X=32 µL	MxP: 15µL
7:	Glucose 20mM * 0.08mL = 100mM * X → X=16 µL	Medium: 1 µL
	Glutamine 20mM* 0.08mL = 50mM * X → X=32 µL	MxP: 15µL
	2-DG 100 mM*0.08mL = 500 mM * X → X=16 µL	
8:	Glucose 20mM * 0.08mL = 100mM * X → X=16 µL	Medium: 15 µL
	Glutamine 20mM* 0.08mL = 50mM * X → X=32 µL	MxP: 15µL

Olygomicin 2µM*80µL = 100 mM * X → X=1.6 µL

3.5 Data Acquisition and Analysis

Raw fluorescence data were acquired as Relative Fluorescence Units (RFU) recorded at each time point for each well. These values represent the absolute extracellular O_2 level in the well at the moment of measurement, as detected by the MitoXpress Xtra probe. Because the probe signal is inversely proportional to O_2 concentration, higher RFU values indicate lower O_2 levels, reflecting greater cellular oxygen consumption. Raw data include contributions from pre-assay cellular respiration and probe equilibration artefacts. To account for thermal equilibration artefacts arising from the transfer of the plate to the reader at 37°C, data acquired during the first 30 minutes of each run were excluded from most of analyses.

Statistical analyses carried out for the experiments are:

Normalised signals (Y/Y_0) were obtained by dividing each time-point value by the first valid reading following the thermal exclusion window, setting this reference point to 1.0 for all conditions. This normalisation removes inter-well variability in absolute fluorescence arising from differences in pipetting volume, local probe concentration, and pre-assay respiratory activity, allowing direct comparison of the relative trajectory of oxygen consumption across experimental groups.

The Oxygen Consumption Rate (OCR) was determined by applying linear regression to the linear portion of each raw fluorescence profile, following the thermal exclusion window and prior to any plateau phase. The slope of the resulting regression line, expressed in RFU/min, represents the instantaneous rate of extracellular oxygen consumption for each individual well, as recommended by the assay manufacturer[19]. Slope values were calculated per individual well prior to averaging across replicates.

For kinetic visualisation purposes, a Savitzky-Golay smoothing algorithm (7-point window) was applied to raw fluorescence traces to reduce technical noise and improve readability of time-course graphs. Smoothing was applied exclusively for graphical representation and had no effect on any quantitative analysis.

All data are expressed as mean ± Standard Error of the Mean (SEM) of three technical replicates ($n = 3$). Statistical comparisons were performed using ordinary two-way Analysis of Variance (ANOVA), with cell line and treatment as independent factors. Post-hoc multiple comparisons were conducted using Sidak's test. A p-value < 0.05 was considered the threshold for statistical significance. For experiments involving a single cell line (A549)

with multiple treatment conditions, a one-way ANOVA was applied, with treatment as the sole independent factor, followed by Sidak's post-hoc test for multiple comparisons. All statistical analyses were performed using GraphPad Prism. All statistical analyses were performed using GraphPad Prism.

4 RESULTS AND DISCUSSION

4.1 Experiment 1

This experiment served as a test platform, not only for the instrument, but also as an understanding of how the cells would respond to the different treatments, and was conducted by initially starving the cells in the free respiration buffer for two hours before running the experiment, leaving them in the incubator after seeding them in the 96-well plate. At the end of the two hours, I added the solution containing the nutrients and performed the reading. The purpose of starving the cells was to make them exhaust their internal reserves, so as to maximize the use of the nutrients provided by the subsequently added solution.

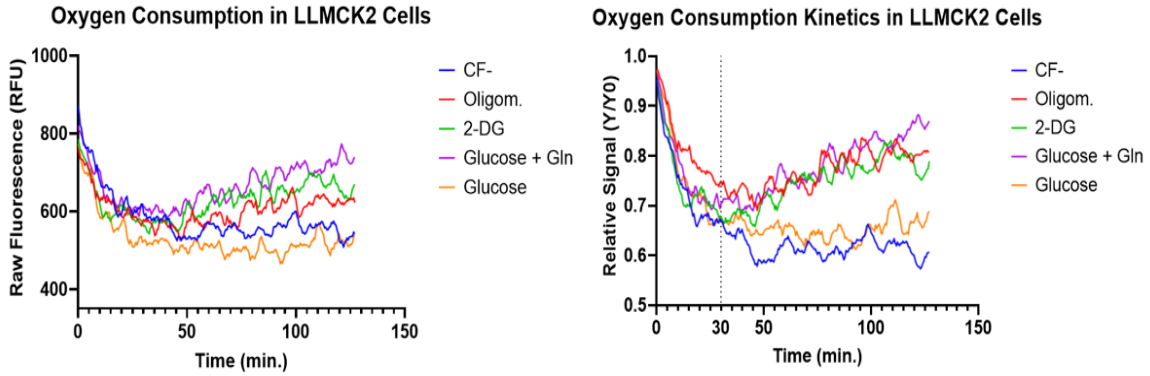

Figure 17 ***Oxygen consumption profiles of LLC-MK2 cells under different metabolic conditions*** *(Left) Smoothed raw fluorescence signal (RFU) over time for LLC-MK2 cells treated with Glucose + Glutamine (GG, 20 mM each), 2-Deoxyglucose (2-DG, 100 mM), Oligomycin (Oligom., 2 µM), Glucose alone (20 mM), and a Cell-Free negative control (CF−). Smoothing was applied using a Savitzky-Golay algorithm (7 points) for visualisation purposes only and does not affect quantitative analysis. (Right) Normalised oxygen consumption signal (Y/Y_0) for the same conditions. Each trace was normalised to its first valid time point, set to 1.0, allowing direct comparison of relative respiratory trajectories independently of inter-well fluorescence variability. The vertical dashed line at t = 30 min indicates the thermal equilibration phase; data within this window are retained for reference but were excluded from quantitative analysis. Data are presented as mean ± SEM of three technical replicates (n = 3). 2-DG: 2-Deoxyglucose; Oligom.: Oligomycin; CF−: cell-free negative control containing culture medium and MitoXpress Xtra probe without cells.*

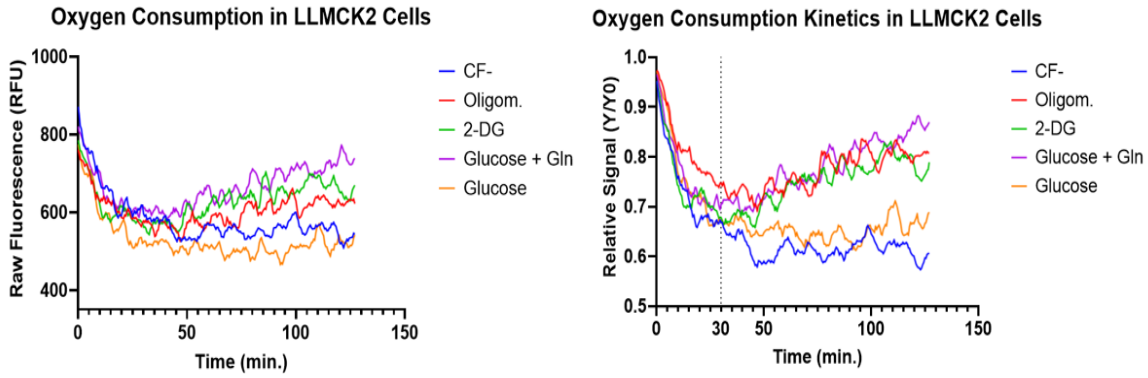

Figure 17, it can be observed how the 2-DG, oligomycin, and glucose plus glutamine lines show higher O_2 consumption compared to the control, without however presenting significant differences between them. Following the characteristics of the LLMCK2, which is an immortalized but non-tumoral cell line, under starvation conditions they do not upregulate the glycolytic pathway but rather remain stable, consuming oxygen, as can be seen from the graph. The trend of the lines in this graph can give an idea of the oxidative phosphorylation behavior in this cell line. For example, it can be seen how glutamine increases O_2 consumption compared to glucose, since glutamine, after being converted to glutamate and entering the Krebs cycle, can provide substrates to oxidative phosphorylation, resulting in an increase in O_2 consumption that is however moderate[9]. It should be noted that the signal increases when extracellular O_2 decreases in the well. The same applies to 2-DG, which, by blocking glycolysis as it is a substrate similar to glucose, leaves the cell with only the oxidative phosphorylation pathway for energy production, thus increasing O_2 consumption. Difficult to explain, on the other hand, is the oligomycin result, which should strongly decrease O_2 consumption. These are preliminary considerations, given that the cell density of the experiment, as we will see from the results of the following experiments, is not sufficient to provide precise explanations of what is happening to cell metabolism; the effect of oligomycin remains to be clarified and will be further investigated in the subsequent experiments.

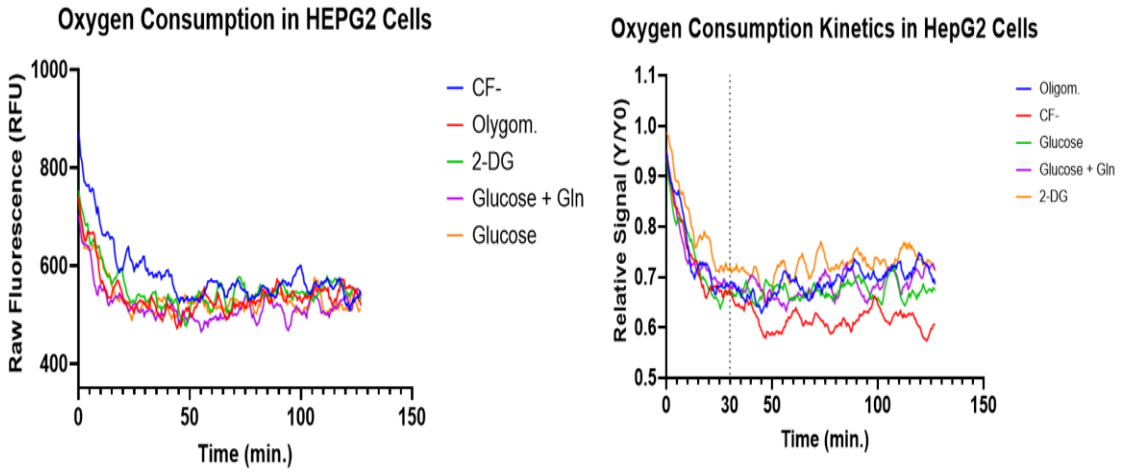

Figure 18 ***Oxygen consumption profiles of HepG2 cells under different metabolic conditions*** *(Left) Smoothed raw fluorescence signal (RFU) over time for HepG2 cells treated with Glucose + Glutamine (GG, 20 mM each), 2-Deoxyglucose (2-DG, 100 mM), Oligomycin (Oligom., 2 µM), Glucose alone (20 mM), and a Cell-Free negative control (CF−). Smoothing was applied using a Savitzky-Golay algorithm (7 points) for visualisation purposes only and does not affect quantitative analysis. (Right) Normalised oxygen consumption signal (Y/Y₀) for the same conditions. Each trace was normalised to its first valid time point, set to 1.0. The vertical dashed line at t = 30 min indicates the thermal equilibration phase; data within this window are retained for reference but were excluded from quantitative analysis. Data are presented as mean ± SEM of three technical replicates (n = 3). 2-DG: 2-Deoxyglucose; Oligom.: Oligomycin; CF−: cell-free negative control containing culture medium and MitoXpress Xtra probe without cells.*

The literature on tumoral cell lines such as HeLa reports that cell starvation decreased oxidative phosphorylation and increased glycolysis; it could be hypothesized that something similar is occurring in this cell line as well[21]. In fact, the responses in *Figure 18* are all nearly equal to the control, with no significant differences among them. The temperature of the plate in these experiments is an important factor, as indicated by the assay manufacturer[19]. In *Figure 18* a signal decrease can be observed during the first 20–30 minutes of analysis; this could be due to a drop in plate temperature during the addition of the solutions, despite these having been pre-warmed. Furthermore, the plastic of the 96-well plate is not impermeable to O_2, which could generate fluctuations in the signal obtained from the TR-F instrument[22,23].

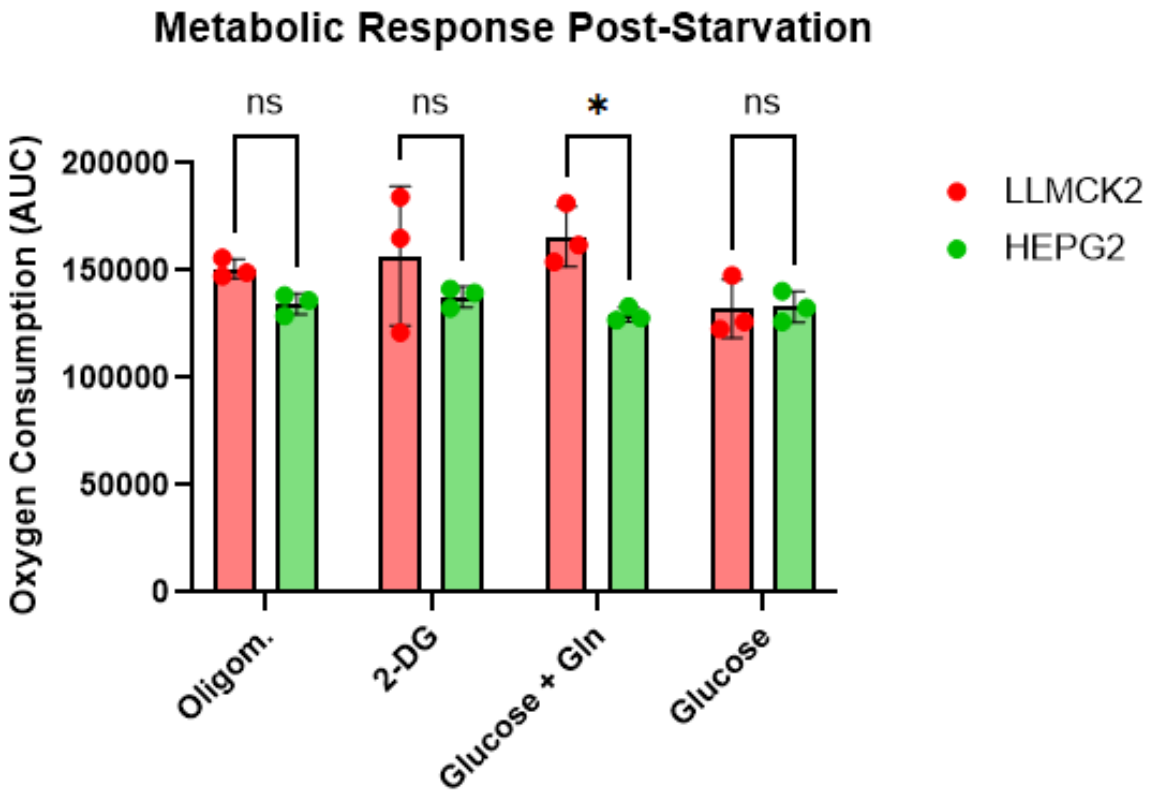

*Figure 19 Metabolic response of normal (LLC-MK2) and tumor (HepG2) cell lines following severe nutrient starvation. Total oxygen consumption was evaluated by calculating the Area Under the Curve (AUC) of the raw fluorescence emission over a 120-minute period. Prior to the assay, cells were subjected to a 2-hour starvation in PBS to induce metabolic stress. Data are expressed as mean ± SD of three independent biological replicates (n=3). Statistical analysis was performed using a Two-way ANOVA followed by Sidak's multiple comparisons test. A statistically significant difference (*p < 0.05) in oxygen consumption was observed between the two cell lines exclusively in the presence of Glucose and Glutamine (Glucose + Gln), highlighting a differential metabolic reliance consistent with the Warburg effect. ns = not significant.*

To quantify the overall respiratory capacity of the two cell lines following nutritional stress, the Area Under the Curve (AUC) was calculated for 129 minutes of analysis (Figure 19). Statistical analysis (Two-way ANOVA) revealed that, under re-feeding conditions with glucose alone, no statistically significant difference in oxygen consumption exists between LLC-MK2 and HepG2 cells. This result is consistent with the severe metabolic arrest induced by prolonged nutrient deprivation, which drove both cell lines toward a minimal basal O_2 consumption[24]. In contrast, the combined administration of glucose and glutamine revealed a significant divergence ($p < 0.05$) between the two cell models. LLC-MK2 cells showed a higher AUC compared to HepG2. Since glutamine is an anaplerotic substrate for the tricarboxylic acid (TCA) cycle, this finding suggests that LLC-MK2 cells maintain marked metabolic flexibility and a strong oxidative coupling capacity (OXPHOS) post-starvation. By contrast, the absence of a respiratory increase in HepG2 cells reflects the

metabolic rigidity typical of the tumoral phenotype (Warburg Effect), in which mitochondrial respiration remains limited even in the presence of optimal substrates[24].

4.2 Experiment 2

The concentrations of experiment 2 were not changed. The instrument settings were changed from "Gain: 176" to "Automatic Gain (optimal)", which notably increased the instrument resolution; in fact, the data from this experiment will be more visible and easier to read. Furthermore, in this experiment the cells were not starved for two hours; after waiting for the overnight attachment time (approximately 24h), the corresponding solutions were added and the analysis was performed.

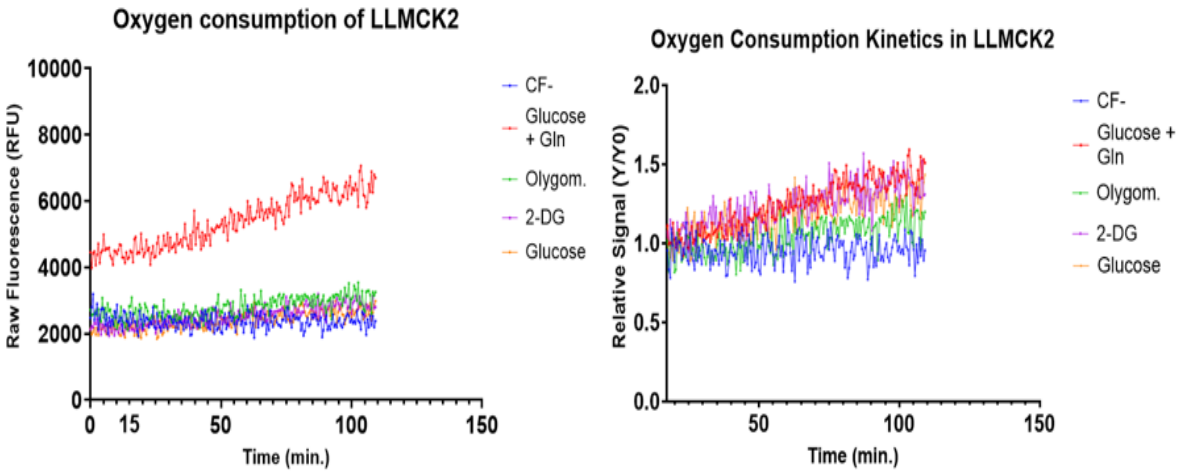

Figure 20 ***Oxygen consumption profiles of LLC-MK2 cells under different metabolic conditions,*** *(Left) Raw fluorescence signal (RFU) recorded over time for LLC-MK2 cells treated with Glucose + Glutamine (GG), Oligomycin (Olygom.), 2-Deoxyglucose (2-DG), Glucose alone (G), and a Cell-Free control (CF−). Data points acquired during the initial thermal equilibration phase (approximately the first 17 minutes) were excluded from analysis to remove the artefactual signal drop caused by plate temperature stabilization from ambient to 37°C. The elevated baseline of the Glucose + Glutamine condition reflects pre-assay respiratory activity occurring during plate sealing and instrument initialization (latency effect). (Right) Normalized oxygen consumption signal (Y/Y_0) for the same conditions. Each trace was normalized to its first valid time point following thermal equilibration (~t = 17 min), set to 1.0, allowing direct comparison of relative respiratory trajectories independently of inter-well fluorescence variability. Data are presented as mean ± SEM of three technical replicates (n = 3). CF−: cell-free negative control containing culture medium and MitoXpress Xtra probe without cells.*

The explanation for why the glutamine line in *Figure 20* starts higher may lie in the fact that, at the moment of medium addition to the 96-well plate, the cells began consuming O_2 rapidly, as also indicated by the trend of this line compared to the others. It cannot be excluded that this phenomenon is due to some factors influenced by pipetting or by the mixing of the

Eppendorf tube, performed by centrifugation, which may have caused uneven substrate distribution or bubble formation, given that the Eppendorf tube containing glutamine was shared among all three cell lines. In fact, in all three cell lines this very high starting point is present, which is not observed in the other experiments. It should be recalled that this is an immortalized, non-tumoral cell line; as already observed, this determines the absence of the Warburg effect in these cells. In *Figure 20* as can be seen from the normalized data (Y/Y0), O_2 consumption is almost similar across all treatments; the lines are around 1.5 (Y/Y0), which demonstrates a high capacity for metabolic regulation under different conditions in order to balance metabolic perturbations. The line showing the lowest consumption is that of oligomycin, which remains around 1.2 (Y/Y0), consistent with the expected pharmacological effect of this compound. In the normalized data, it can also be seen how 2-DG influenced respiration, which appears slightly higher than glucose.

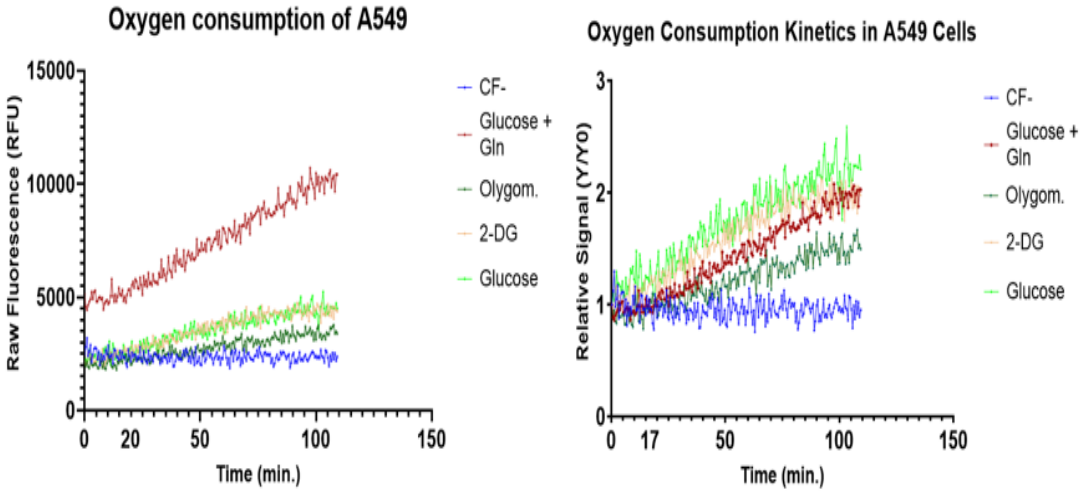

Figure 21 ***Oxygen consumption profiles of A549 cells under different metabolic conditions*** *(Left) Raw fluorescence signal (RFU) recorded over time for A549 cells treated with Glucose + Glutamine (GG), Oligomycin, 2-Deoxyglucose (2-DG), Glucose alone, and a Cell-Free control (CF−). Data points acquired during the initial thermal equilibration phase (approximately the first 17 minutes) were excluded from analysis to remove the artefactual signal drop caused by plate temperature stabilisation from ambient to 37°C. The elevated baseline of the Glucose + Glutamine condition reflects pre-assay respiratory activity occurring during plate sealing and instrument initialisation (latency effect). (Right) Normalised oxygen consumption signal (Y/Y_0) for the same conditions. Each trace was normalised to its first valid time point following thermal equilibration (~t = 17 min), set to 1.0, allowing direct comparison of relative respiratory trajectories independently of inter-well fluorescence variability. Data are presented as mean ± SEM of three technical replicates (n = 3). CF−: cell-free negative control containing culture medium and MitoXpress Xtra probe without cells.*

In *Figure 21*, the starting point of the glutamine line has already been explained in the previous graph. The effect of oligomycin as an inhibitor of complex V of oxidative phosphorylation is confirmed, resulting in low O_2 consumption. It can be seen that the metabolic activity of this cell line is much higher compared to the previous cell line, as will also be observed for the HepG2 line. The lines in the normalized *Figure 21* show a solid 2.0 for treatments such as glucose, 2-DG and glutamine, with sustained O_2 consumption; this demonstrates a bivalent behavior of this cell line[25] which, under conditions of medium acidosis produced by the Warburg effect, shifts its metabolism favoring oxidative phosphorylation. No comparison method with lactic acid production is available to determine which metabolic pathway is

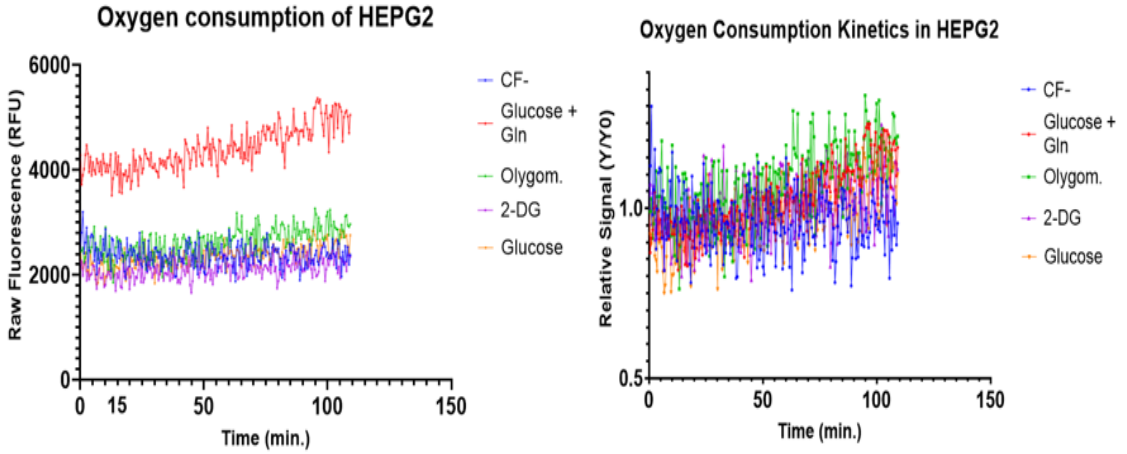

Figure 22 Oxygen consumption profiles of HepG2 cells under different metabolic conditions (Left) Raw fluorescence signal (RFU) recorded over time for HepG2 cells treated with Glucose + Glutamine (GG), Oligomycin (Olygom.), 2-Deoxyglucose (2-DG), Glucose alone, and a Cell-Free control (CF−). Data points acquired during the initial thermal equilibration phase (approximately the first 17 minutes) were excluded from analysis to remove the artefactual signal drop caused by plate temperature stabilisation from ambient to 37°C. The elevated baseline of the Glucose + Glutamine condition reflects pre-assay respiratory activity occurring during plate sealing and instrument initialisation (latency effect). (Right) Normalised oxygen consumption signal (Y/Y_0) for the same conditions. Each trace was normalised to its first valid time point following thermal equilibration (~t = 17 min), set to 1.0, allowing direct comparison of relative respiratory trajectories independently of inter-well fluorescence variability. Following normalisation, all conditions remain clustered around the baseline value of 1.0 throughout the observation window, with no sustained increase in oxygen consumption detectable under any treatment.

In this cell line, it is evident from *Figure 22* that O_2 consumption is much lower compared to the other tumoral cell line A549. The lines stop around 1.0 (Y/Y0), which would suggest that oxidative phosphorylation is essentially switched off a strong confirmation of the

Warburg effect. Based on the literature, this cell line in the presence of glucose is strongly driven to use glycolysis rather than oxidative phosphorylation[24]. The fact that, even for this cell line, which overall does not show O_2 consumption as high as the other cell lines, the glutamine line is higher than the others would suggest some instrumental artifact due to the operator or to pipetting, consolidating the hypothesis of an operator-dependent artifact.

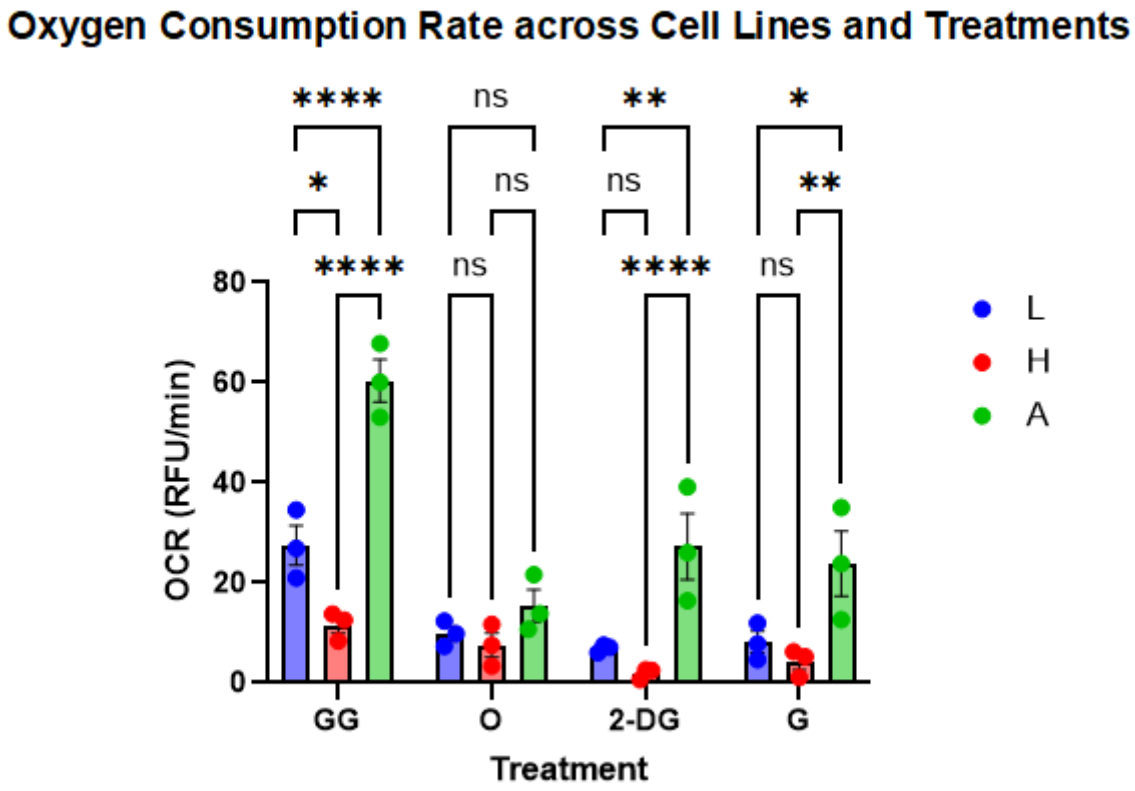

Figure 23 ***Oxygen Consumption Rate (OCR) of LLC-MK2, HepG2, and A549 cells under different metabolic conditions*** *OCR was calculated as the slope of the linear portion of the raw fluorescence signal (t = 45–100 min) by simple linear regression, following exclusion of data acquired during the thermal equilibration phase. Data are presented as mean ± SEM of three technical replicates (n = 3). Statistical analysis was performed by two-way ANOVA followed by Sidak's multiple comparisons test. Significance thresholds: * $p < 0.05$, ** $p < 0.01$, **** $p < 0.0001$; ns = not significant. L: LLC-MK2; H: HepG2; A: A549. GG: Glucose + Glutamine; O: Oligomycin; 2-DG: 2-Deoxyglucose; G: Glucose.*

Figure 23 shows the OCR of the different cell lines; based on the slope of the lines, the rate at which extracellular O_2 is consumed can be extrapolated. It is very evident that the HepG2 line shows the lowest O_2 consumption, confirming what was observed in the analysis of the individual cell line, with a very evident Warburg effect. This is followed by the LLC-MK2 line, which maintains the behavior of a normal cell, and then the A549 line, which, contrary

to what might be expected, despite being a tumoral cell line, shows a very high O_2 consumption rate with low reliance on the Warburg effect[25]. It can be noted that the effect of 2-DG does not increase O_2 consumption as would be expected; a search of the literature did not return extensive information regarding the cell lines used in this study.

4.3 Experiment 3

The core of this experiment was based on understanding which glutamine concentration was most effective in the three cell lines. Each well contained a base glucose concentration of 20 mM, to which increasing concentrations of glutamine were added: 1 mM, 10 mM and 20 mM. Unlike the other experiments, glutamine, a stimulator of oxidative phosphorylation, served as the baseline in the medium used to perform the analysis, to which the relevant compounds were then added to highlight their efficacy. This approach may have increased the visibility of the effects of each compound. These tests were performed in triplicate for each cell line, as in the other experiments and those to follow. For an analysis of the efficacy of glutamine concentration, the A549 cell line was selected, given that it has the fastest metabolism and should best highlight the differences among the various concentrations. LLC-MK2 and HepG2 did not show differences significant enough to drive a choice. Furthermore, modifications were made to this experiment regarding cell density, increased from 60,000 to 80,000 cells per well, and the MitoXpress probe, increased from 10 µL to 15 µL; all of this was aimed at improving the resolution of the lines, an objective only partially achieved. As will be evident in Experiment 6, the resolution will improve further, making the true metabolic trend much more readable.

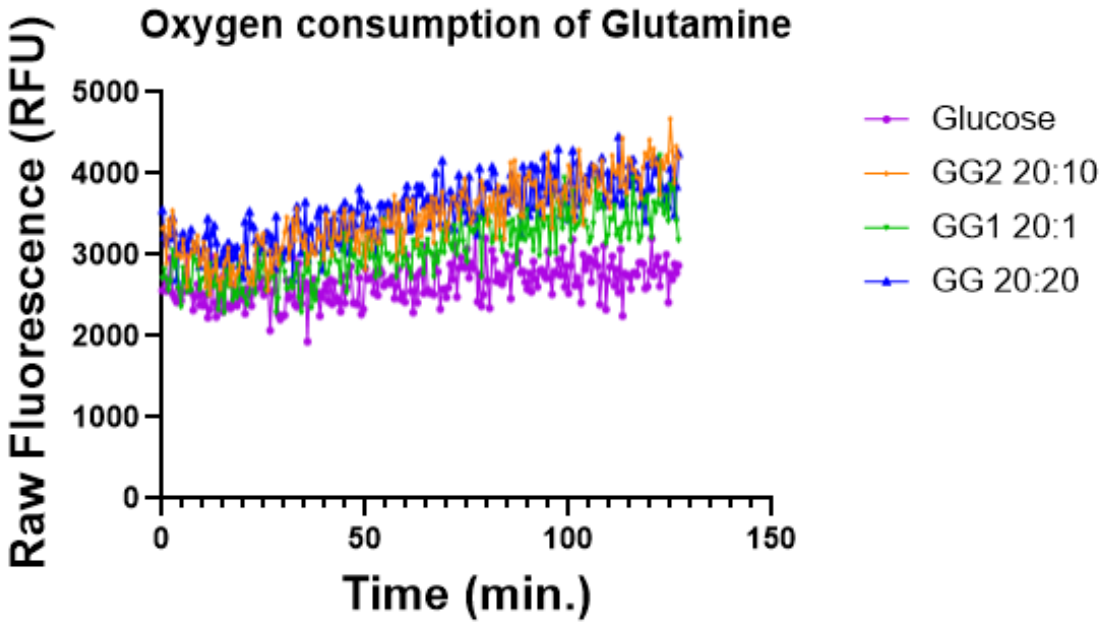

Figure 24 ***Effect of increasing glutamine concentrations on oxygen consumption in A549 cells*** *Raw fluorescence signal (RFU) over time for A549 cells treated with Glucose alone (20 mM) or Glucose + Glutamine at three different glutamine concentrations: 1 mM (GG1 20:1), 10 mM (GG2 20:10), and 20 mM (GG 20:20), all with a fixed glucose concentration of 20 mM. Data are presented as mean ± SEM of three technical replicates (n = 3) and include the full time course without exclusion of the initial thermal equilibration phase. GG: Glucose + Glutamine; the numerical ratio indicates glucose-to-glutamine molar concentration (mM:mM).*

In order to evaluate the best glutamine concentration for the subsequent experiments so as to obtain the best response, the different concentrations were compared in a single cell line. This experiment did not provide a clear answer; in fact, the lines in Figure 24 are all close to one another. A glutamine concentration of 20 mM was therefore arbitrarily selected, given the absence of significant differences among the tested concentrations; from this point on, only the wells with that glutamine concentration will be taken into consideration. The other results of this experiment are not significant for the purpose of extracting further information beyond what was already obtained from the previous ones. This experiment therefore remains useful for the determination of the glutamine concentration.

4.4 Experiment 4

In this experiment, a new compound was used, namely FCCP, a compound also indicated in the Agilent operator manual to drastically increase O_2 consumption. A MitoXpress concentration of 15 µM was maintained. Furthermore, the HepG2 cell line was deliberately excluded, given that it did not show any response throughout the previous experiments; the growth times required to reach the minimum cell density for seeding in the 96-well plate were very long, and it was therefore excluded. Additionally, this experiment aimed to evaluate the most suitable cell density in order to obtain better results. Two different FCCP concentrations were evaluated: 1 µM and 2.5 µM. Furthermore, due to an instrument settings error, only data for the A549 cell line is available, as those regarding LLC-MK2 are incomplete. Additionally, lactate was used at the same concentration as glucose, equal to 20 mM, to assess whether it could influence O_2 consumption. In the next experiment, lactate will be compared with glutamine.

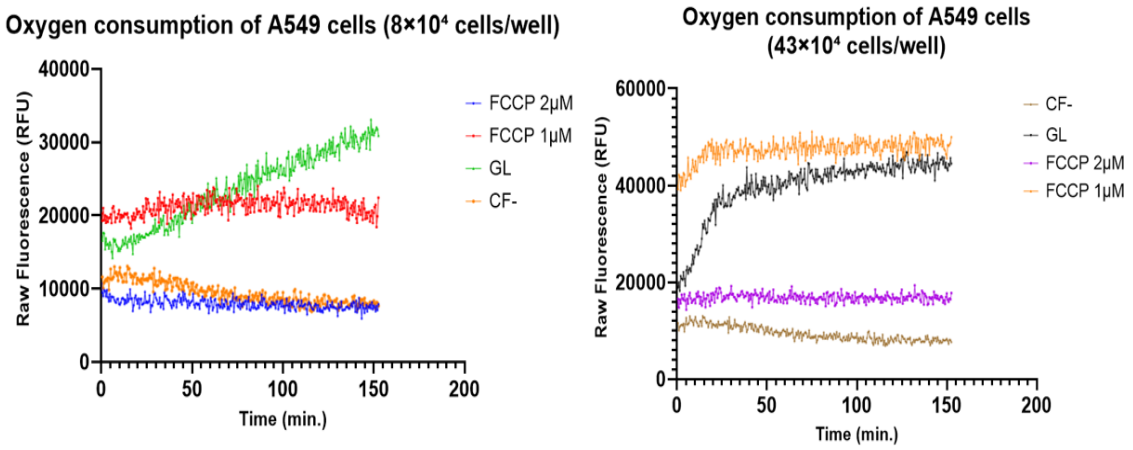

Figure 25 ***Oxygen consumption of A549 cells at two seeding densities treated with Glucose + Lactate and FCCP*** *Raw fluorescence signal (RFU) over time for A549 cells seeded at 8×10⁴ cells/well (left) and 43×10⁴ cells/well (right), treated with Glucose + Lactate (GL, 20 mM each) or FCCP (carbonyl cyanide 4-(trifluoromethoxy)phenylhydrazone) at 1 µM and 2 µM, alongside a Cell-Free negative control (CF−). Data include the full time course without exclusion of the initial thermal equilibration phase. Data are presented as mean ± SEM of three technical replicates (n = 3). GL: Glucose + Lactate; FCCP: carbonyl cyanide 4-(trifluoromethoxy)phenylhydrazone; CF−: cell-free negative control containing culture medium and MitoXpress Xtra probe without cells.*

Analyzing the signals from Figure 25 starting from FCCP at a concentration of 2 µM, it can be stated that there was probably some instrumental error, as in the previous experiment regarding pipetting or centrifugation, which altered the result. It can be excluded that this is

a biological effect, as in the next experiment it will be shown how the different FCCP concentrations will not cause this type of trend. Comparing the lines in this graph, it is evident that a higher density yields a qualitatively better response. The O_2 consumption in the wells involved in the experiment is in fact clearly visible; FCCP rapidly increases consumption until reaching a plateau of approximately 46,000 RFU, evident in the higher-density plates, while the result in the lower-density plates is much more modest and difficult to interpret. The effect of FCCP increases O_2 consumption to a greater extent compared to the glucose plus lactate wells. The aim of evaluating the most suitable cell density for future experiments was achieved: the density will need to be drastically increased.

4.5 Experiment 5

This was the best experiment among all those performed up to this point; the knowledge gained from the previous ones, regarding cell density values, suitable MitoXpress concentrations, and the concentrations of the studied compounds, led to well-defined resolutions and clearly separated lines. The LLC-MK2 line is not present due to a settings error in the instrument, which compromised the relevant wells.

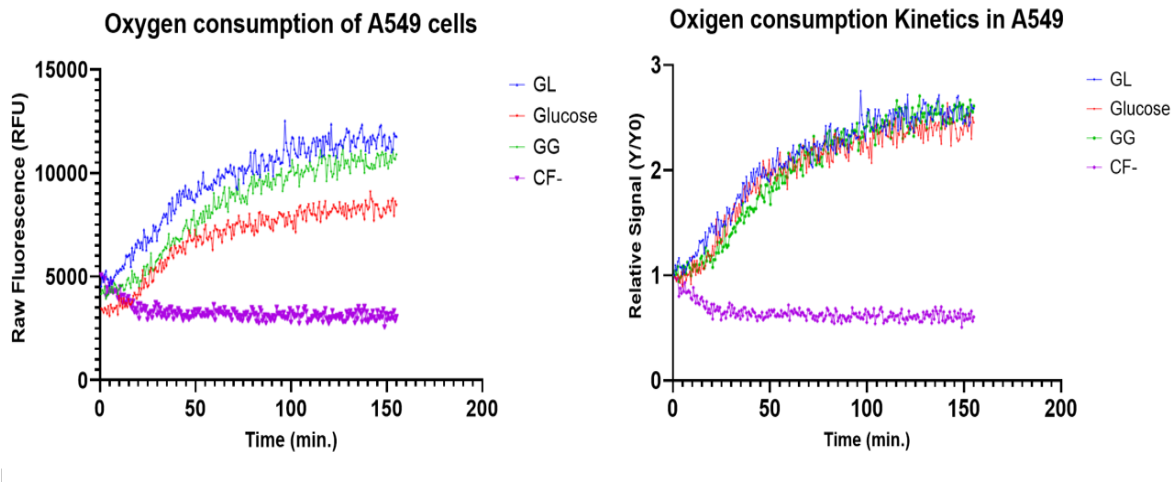

Figure 26 ***Oxygen consumption of A549 cells (2.5×10⁵ cells/well) under different carbon source conditions.*** *(Left) Raw fluorescence signal (RFU) over time for A549 cells treated with Glucose + Lactate (GL, 20 mM each), Glucose + Glutamine (GG, 20 mM each), Glucose alone (20 mM), and a Cell-Free negative control (CF−). Data include the full time course without exclusion of any preliminary time window. (Right) Normalised oxygen consumption signal (Y/Y₀) for the same conditions. Each trace was normalised to its first valid time point, set to 1.0, allowing direct comparison of relative respiratory trajectories independently of inter-well fluorescence variability. Data are presented as mean ± SEM of three technical replicates (n = 3). GL: Glucose + Lactate; GG: Glucose + Glutamine; CF−: cell-free negative control containing culture medium and MitoXpress Xtra probe without cells.*

In Figure 26 it can be seen how the influence of lactate and glutamine leads to a higher O_2 consumption compared to glucose, but with the same trend, as shown by the normalized data. Only the carbon sources were evaluated in order to compare them with one another, without the influence of other compounds that would cause much larger variations in metabolism. These will be evaluated subsequently in the same experiment.

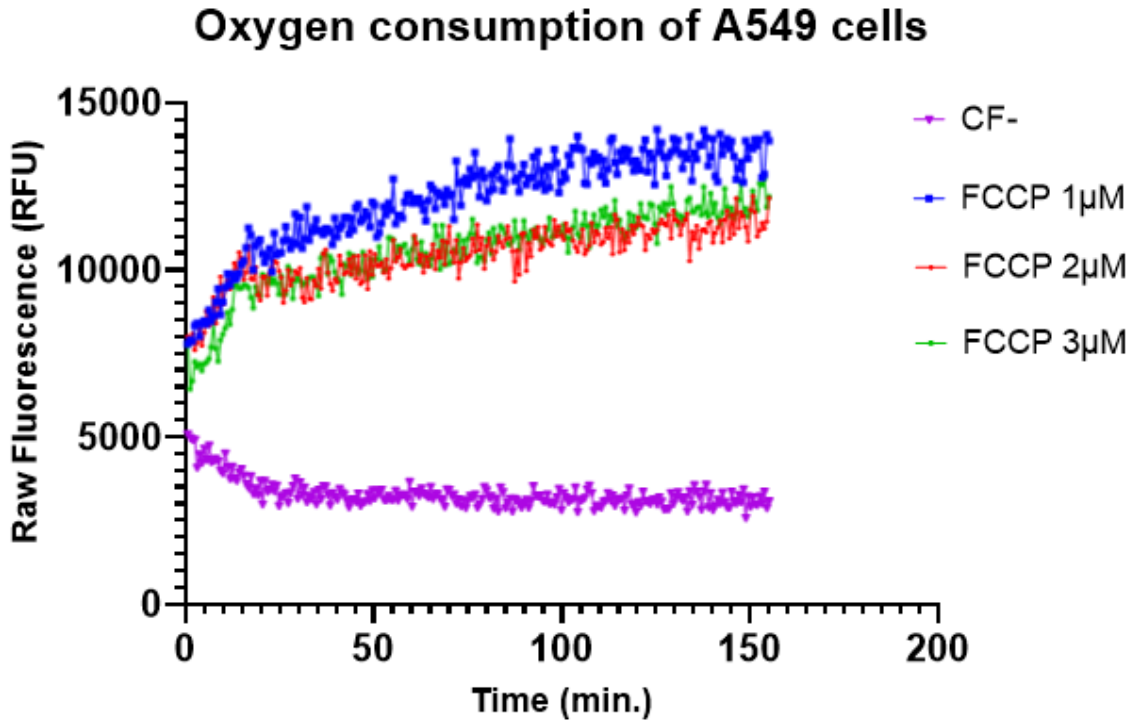

Figure 27 ***Oxygen consumption of A549 cells (2.5×10⁵ cells/well), FCCP dose-response.*** *Raw fluorescence signal (RFU) over time for A549 cells treated with FCCP (carbonyl cyanide 4-(trifluoromethoxy)phenylhydrazone) at 1 µM (F1), 2 µM (F2), and 3 µM (F3), alongside a Cell-Free negative control (CF−). Data include the full time course without exclusion of any preliminary time window. Data are presented as mean ± SEM of three technical replicates (n = 3).*

This compound leads to a very rapid increase in O_2 consumption, as shown by the initial rise of the curve in Figure 27. These wells were used to evaluate which FCCP concentration would be best to use in the comparison with the other compounds and in the construction of the mathematical model. FCCP was used at a concentration of 1 µM, determined by scalar titration (1, 2, 3 µM). This concentration elicited the maximum oxygen consumption, consistent with complete mitochondrial uncoupling. Higher concentrations produced a reduced fluorescence signal, indicating mitochondrial toxicity at supra-optimal doses.[19].

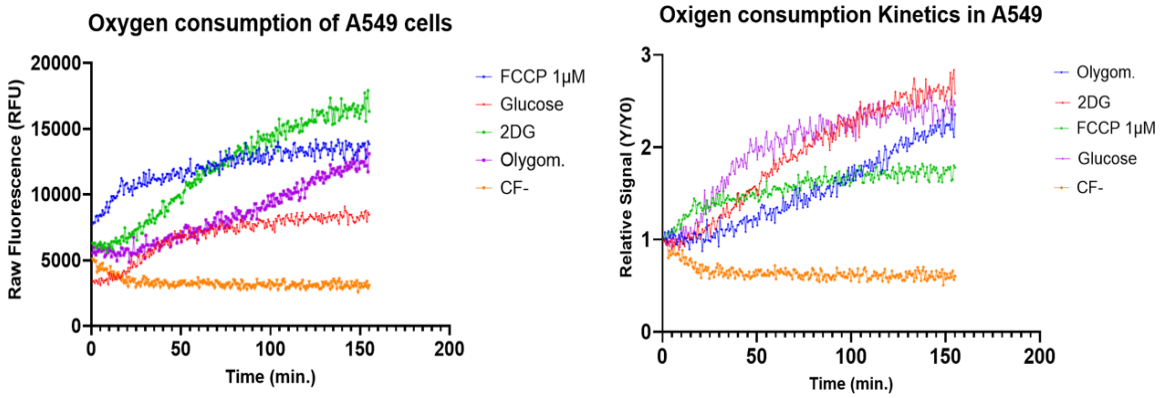

Figure 28 ***Oxygen consumption of A549 cells (2.5×10⁵ cells/well) under pharmacological modulation of energy metabolism.*** *(Left) Raw fluorescence signal (RFU) over time for A549 cells treated with FCCP at 1 µM (carbonyl cyanide 4-(trifluoromethoxy)phenylhydrazone), 2-Deoxyglucose (2-DG, 100 mM), Oligomycin (Oligom., 2 µM), Glucose alone (20 mM), and a Cell-Free negative control (CF−). Data include the full time course without exclusion of any preliminary time window. (Right) Normalised oxygen consumption signal (Y/Y₀) for the same conditions. Each trace was normalised to its first valid time point, set to 1.0, allowing direct comparison of relative respiratory trajectories independently of inter-well fluorescence variability. Data are presented as mean ± SEM of three technical replicates (n = 3). FCCP: carbonyl cyanide 4-(trifluoromethoxy)phenylhydrazone; 2-DG: 2-Deoxyglucose; Oligom.: Oligomycin; CF−: cell-free negative control containing culture medium and MitoXpress Xtra probe without cells.*

In Figure 28 it can be clearly seen how oligomycin slows down metabolism by blocking oxidative phosphorylation; it is in fact the least steep curve of all. The 2-DG line reaches, by the end of the experiment, a higher O_2 consumption than all the others; extending the experiment would have helped to understand how far the O_2 consumption curve could rise. Glucose in Figure 28 serves as a control, representing the basal O_2 consumption of the A549 cell line in the absence of metabolic perturbations.

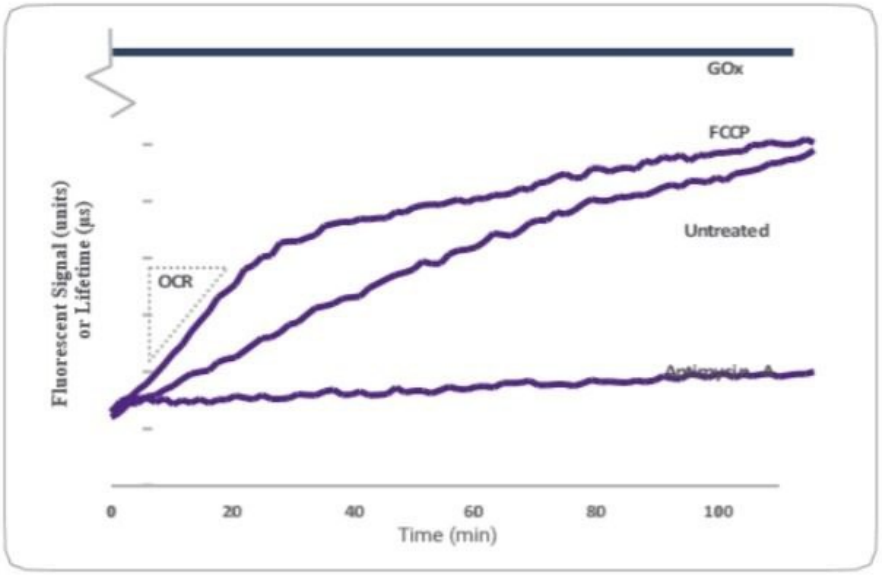

Figure 29 Representative oxygen consumption profiles of cells treated with different mitochondrial modulators, as measured by MitoXpress fluorescent probe. The slope of the linear phase (indicated by the dashed box) corresponds to the OCR. Adapted from: Agilent MitoXpress Xtra Assay Manual[19].

Figure 29 shows how, in the manufacturer's manual, the lines appear very similar to those obtained in Figure 28, particularly the line regarding FCCP. Furthermore, Figure 29 shows which portion of the line is used to calculate the OCR, corresponding to the same portion used for the calculation relative to the FCCP line in Figure 28.

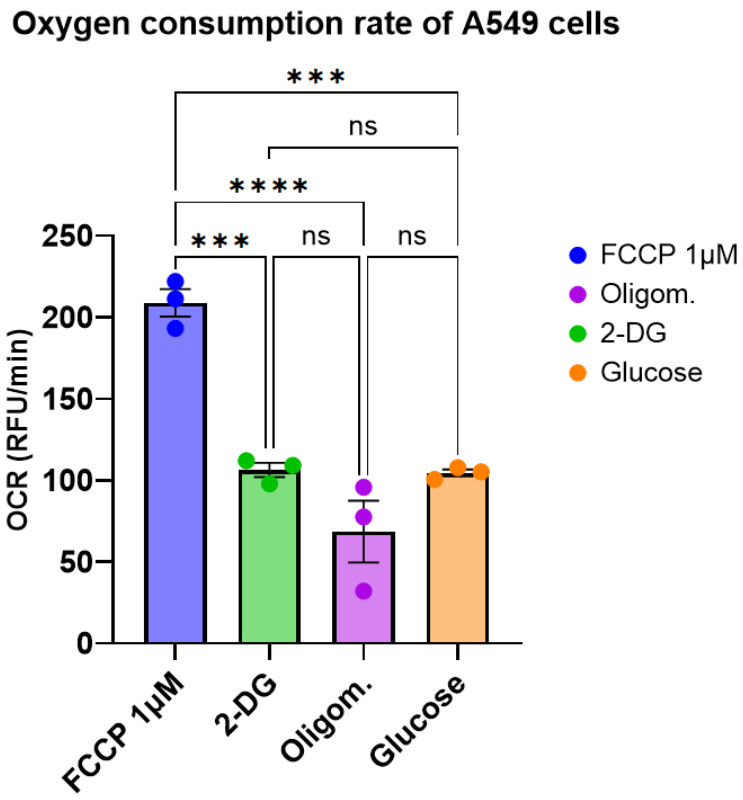

Figure 30 ***Oxygen consumption rate (OCR) of A549 cells under different metabolic conditions,*** *bar graph showing mean OCR (RFU/min) ± SEM of A549 cells treated with FCCP (1 µM), 2-deoxy-D-glucose (2-DG, 100 mM), oligomycin (2 µM), or glucose alone (20 mM). OCR was calculated as the slope of the linear phase of the raw fluorescence signal over condition-specific time windows: FCCP (t = 0–15 min), 2-DG (t = 18–100 min), oligomycin (t = 30–150 min), and glucose (t = 10–45 min). Individual data points represent technical replicates (n = 3). Statistical analysis: One-way ANOVA with Sidak's post-hoc test. **** p < 0.0001. ns = not significant. OCR: oxygen consumption rate; FCCP: carbonyl cyanide 4-(trifluoromethoxy)phenylhydrazone; 2-DG: 2 deoxy-D-glucose.*

The Figure 30 shows the OCR (oxygen consumption rate) of A549 cells under four treatment conditions. FCCP 1 µM presents the highest value (~207 RFU/min), significantly higher than all other conditions ($p < 0.0001$). 2-DG (~106 RFU/min) and glucose (~104 RFU/min) show practically identical values, while oligomycin records the lowest value (~86 RFU/min). No statistically significant difference is observable among 2-DG, oligomycin and glucose.

4.6 Mathematical model in Mathlab

The model in Figure 32 was built starting from the model by Nitin Patil and Zoreh Mirvais[9,20], using the software MATLAB, in particular the program SIMBIOLOGY. In this project, the section regarding oxidative phosphorylation was added, comprising the components O_2, O_2_ex, capacity_O_2, OxPP and FCCP, as also indicated by the assay manufacturer's manual[19], which will be explained later in this paragraph. In general, this mathematical model was built based on ordinary differential rate equations that aim to replicate cell metabolism as a function of the components placed outside the cell. In this text, oxidative phosphorylation will be addressed; the other metabolic pathways have been described in the papers by Nitin Patil and Zoreh Mirvais with the respective models adapted to their experiments. The addition of these compounds modifies the model output according to equilibrium constants, represented by each yellow circle, which acts as a junction between an external compartment and an internal one and vice versa, and the key reactions within the cell. The simplification of the model concerns approximations necessary for the purposes of this study, given that no data were available regarding the specific internal processes of cell metabolism.

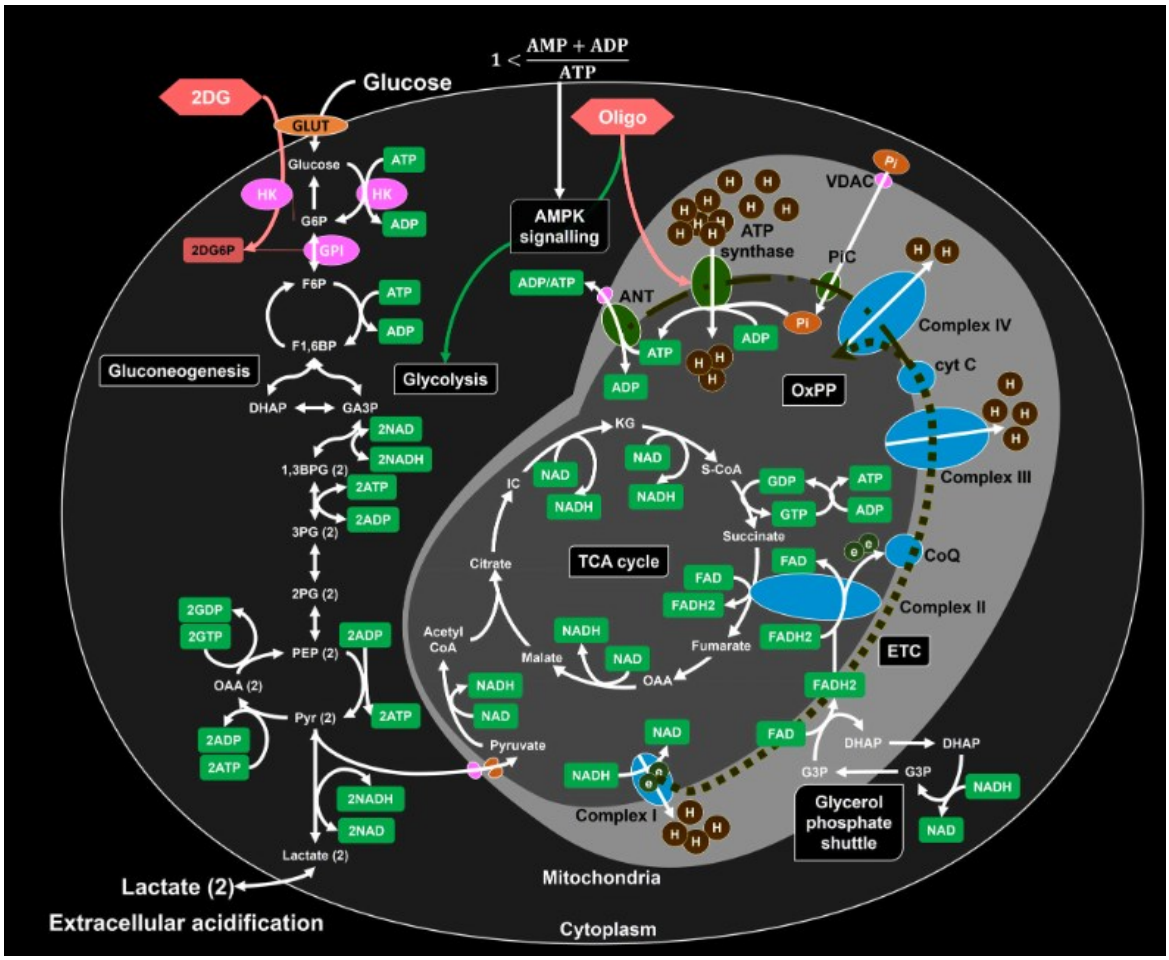

Figure 31 ***Overview of cellular glucose metabolism and pharmacological modulation sites*** *Schematic representation of the central carbon metabolic pathways in a eukaryotic cell. Glucose is taken up via glucose transporters (GLUT) and catabolised to pyruvate through glycolysis in the cytoplasm. Pyruvate can either be reduced to lactate — contributing to extracellular acidification — or enter the mitochondria to fuel the tricarboxylic acid (TCA) cycle and the electron transport chain (ETC), culminating in oxidative phosphorylation (OxPP) and maximal ATP yield. Under conditions of energy scarcity (AMP+ADP/ATP > 1), the AMPK signalling pathway is activated, stimulating glycolytic flux. The sites of action of the two pharmacological modulators used in this study are indicated: 2-deoxyglucose (2DG) inhibits hexokinase (HK) and glucose-6-phosphate isomerase (GPI) at the first step of glycolysis, while oligomycin (Oligo) blocks ATP synthase, inhibiting mitochondrial ATP production. Adapted from Patil et al., FEBS Open Bio, 2024*[20].

In Figure 31 can be seen that the cellular pathways are numerous and complex, and the simplification highlights the main junction points of cell metabolism, namely the yellow circles in Figure 32. This simplification was also functional to the purpose; in fact, the aim was to provide a simple analytical method for any cell line using commercial tools such as MitoXpress or pH-Xtra glycolysis assay for ECAR measurement (Agilent)[26]. The final goal of the model was to provide a predictive tool that could be freely modulated by inserting any type of compound to modify cell metabolism, and therefore monitor any cell line, observing how the different compounds would modify their metabolism in order to generate the desired predictions.

4.6.1 Structure of the model

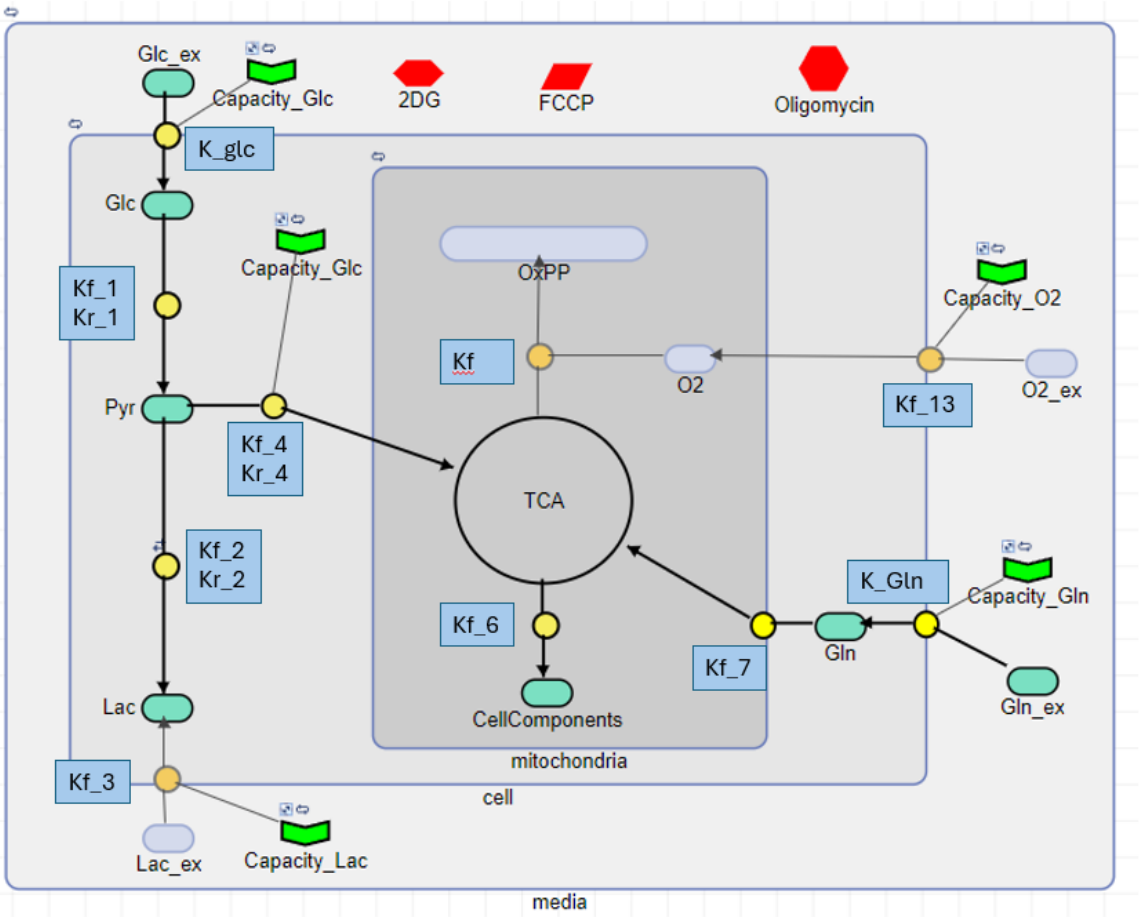

Figure 32 ***Schematic representation of the kinetic model of oxygen consumption in A549 cells*** *The model was developed in MATLAB SimBiology and is based on ordinary differential rate equations (ODEs). Model components (teal) are connected through reaction blocks (yellow circles) according to their metabolic pathway and cellular localisation. The media compartment contains the extracellular reservoirs of glucose (Glc_ex), glutamine (Gln_ex), lactate (Lac_ex) and oxygen (O2_ex), each regulated by a pathway capacity (Capacity_Glc, Capacity_Gln, Capacity_Lac, Capacity_O2) acting as a boundary condition to prevent uncontrolled substrate flooding. In the cytoplasmic compartment, extracellular glucose enters the cell at rate K_glc and is reversibly catabolised to pyruvate (Pyr; kf_1/kr_1), which can either be reversibly converted to lactate (Lac; kf_2/kr_2) or enter the mitochondrial TCA cycle (kf_4/kr_4). Extracellular glutamine (Gln_ex) enters the cell at rate K_Gln and feeds the TCA cycle directly (kf_7). Within the mitochondrial compartment, TCA cycle flux is directed either towards CellComponents (kf_6) or towards oxidative phosphorylation (OxPP), the latter consuming intracellular oxygen (O2; rate kf) in a reaction modulated by oligomycin and FCCP. Extracellular lactate is transported out of the cell at rate kf_3, regulated by Capacity_Lac. The three pharmacological modulators — 2-deoxyglucose (2DG), FCCP, and oligomycin — are represented by red hexagons and act at their respective nodes as described in the text. Forward and reverse rate constants (kf, kr) were optimised by data fitting to experimental MitoXpress fluorescence profiles.*

The cell in the model in Figure 32 is represented by the "cell" compartment, which contains the glycolysis reactions from external glucose (GLC_ex) to pyruvate (PYR), which enters the Krebs cycle (TCA), through to external lactate (LAC_ex). The cell also includes the internal mitochondrial compartment (mitochondria), where the oxidative phosphorylation

icon is present, grouped into a single unit (OxPP), influenced by the entry of O_2 from outside, regulated by the yellow circle with an equilibrium constant that will be discussed later. The glutamine pathway (GLN_ex) is also represented, entering the Krebs cycle. Finally, the culture medium contains the compounds added as needed for both cell growth and the success of the experiments, namely glucose, glutamine, FCCP, oligomycin and 2-DG; this compartment is referred to as "media" (DMEM Sigma Aldrich D5030-HEPPS). The icons labeled "Capacity" incorporated in the equations act as gates that limit the entry of compounds when the internal concentration reaches the established threshold, preventing excessive uptake into the cell. These were inserted at the glucose entry, lactate exit and oxygen entry points.

```
1  Reaction_1 = k_Glc*Glc_ex*(media.Capacity_Glc)
2  Reaction_2 = kf_1*Glc*(1-[2DG]*i2)-kr_1*Pyr
3  Reaction_3 = kf_2*Pyr-kr_2*Lac
4  Reaction_4 = kf_3*Lac
5  Reaction_5 = kf_4*Pyr-kr_4*(TCA)
6  Reaction_6 = kf_6*TCA*(1-[2DG]*i2)
7  Reaction_7 = k_Gln*Gln_ex*Capacity_Gln
8  Reaction_8 = kf_7*Gln
9  Reaction_10 = kf*TCA*O2*(1-Oligomycin*i1)*(1+FCCP*s1)
10 Reaction_9 = kf_13*O2_ex*Capacity_O2
```

Figure 33 ***Ordinary differential rate equations governing the kinetic model of oxygen consumption in A549 cells.*** *Each reaction describes the rate of transition between model species according to their metabolic role. Reaction_1: glucose uptake from the extracellular reservoir, regulated by Capacity_Glc. Reaction_2: reversible conversion of glucose to pyruvate, inhibited by 2-DG at rate i2. Reaction_3: reversible conversion of pyruvate to lactate. Reaction_4: irreversible export of lactate to the extracellular compartment. Reaction_5: reversible entry of pyruvate into the mitochondrial TCA cycle. Reaction_6: irreversible flux from TCA cycle towards CellComponents, inhibited by 2-DG at rate i2. Reaction_7: glutamine uptake from the extracellular reservoir, regulated by Capacity_Gln. Reaction_8: irreversible entry of glutamine into the TCA cycle. Reaction_10: irreversible flux from TCA cycle towards oxidative phosphorylation (OxPP), consuming intracellular O2, inhibited by oligomycin at rate i1 and stimulated by FCCP at rate s1. Reaction_9: oxygen uptake from the extracellular reservoir, regulated by Capacity_O2. kf, forward rate constant; kr, reverse rate constant; i1, oligomycin inhibition rate; i2, 2-DG inhibition rate; s1, FCCP stimulation rate; 2-DG, 2-deoxy-D-glucose; FCCP, carbonyl cyanide 4-(trifluoromethoxy)phenylhydrazone; TCA, tricarboxylic acid cycle; OxPP, oxidative phosphorylation pathway*

In Figure 33, the various equilibrium constants are indicated, which regulate not only the entry of components into the cell but also the various conversion reactions. It can be seen how oligomycin, 2-DG and FCCP are incorporated into these equations with inhibition constants,

so that when one pathway is suppressed, another is upregulated. Below are the equilibrium constants of the reactions in the model in Figure 34; these produce as output the lines that will be explained later.

$K\_glc \ = \ 1.2 * 10^{-4}$

$Kf\_1 = 1$

$Kr\_1 = 0.01$

$K\_i2\ (2\_DG) \ = 0.01$

$Kf\_2 \ = 1$

$Kr\_2 = 0.100$

$Kf\_3 = 0.100$

$Kf\_4 = 0.17$

$Kr\_4 = 0.01$

$Kf\_6 = 0.05$

$K\_i2\ (2 - DG) \ = 0.01$

$Kf\_7 = 0.500$

$K\_Gln = 0.9$

$Kf\_13 = 1.0 * 10^{-3}$

$Kf\ (referring\ to\ the\ output\ of\ oxidative\ phosphorylation) = 0.01$

$Ki\_1\ (Olygomicin) = 0.1$

$Ks\_1\ (FCCP) \ = \ 100$

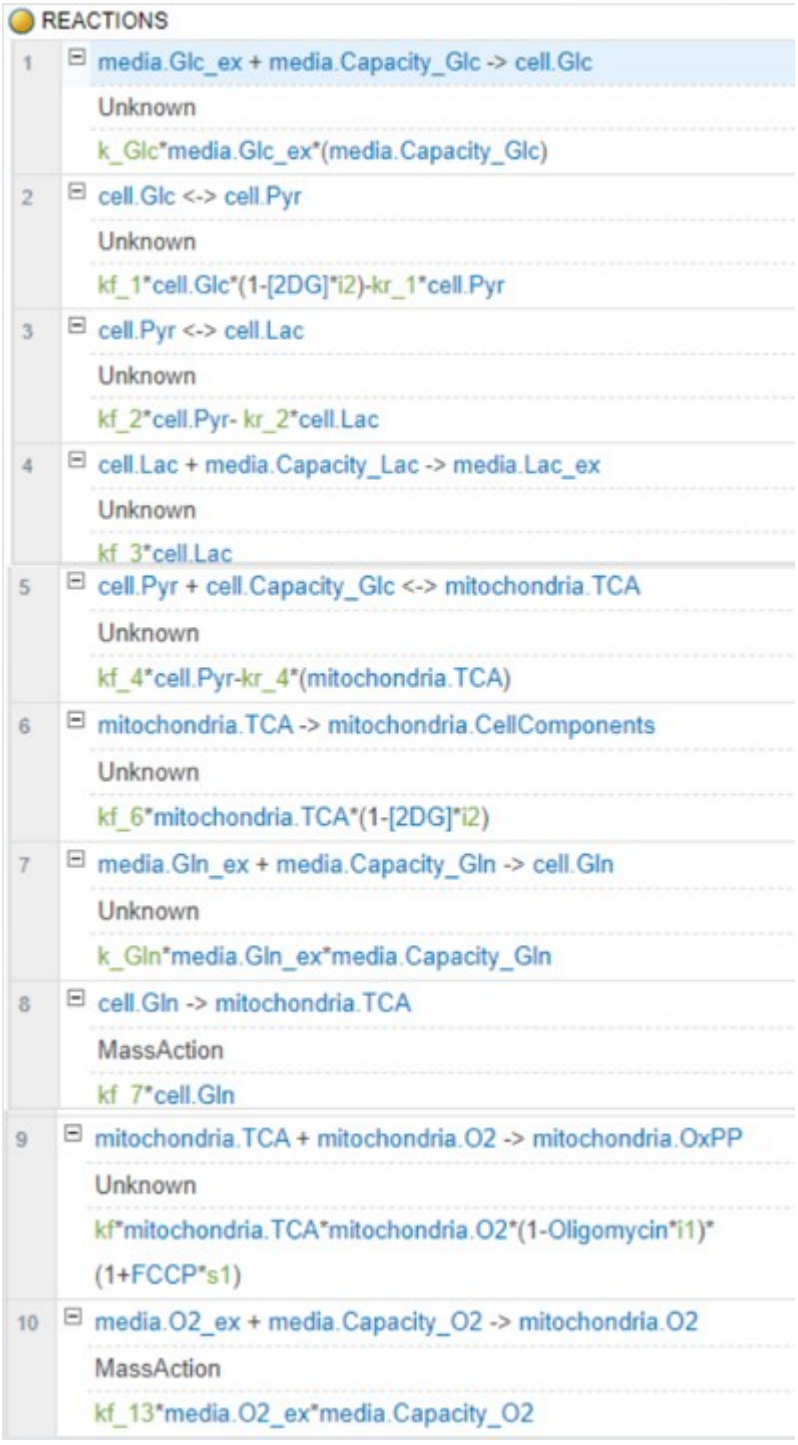

Figure 34 ***Reaction scheme of the kinetic model of oxygen consumption in A549 cells as implemented in MATLAB SimBiology, f****or each reaction, the compartmental localisation of reactants and products, the reversibility, and the corresponding rate equation are shown. Reactions 1 and 7 describe the uptake of extracellular glucose (Glc_ex) and glutamine (Gln_ex) into the cell, regulated by their respective pathway capacities (Capacity_Glc, Capacity_Gln). Reaction 2 describes the reversible conversion of intracellular glucose to pyruvate, inhibited by 2-DG at rate i2. Reaction 3 describes the reversible interconversion of pyruvate and lactate. Reaction 4 describes the irreversible export of lactate to the extracellular compartment, regulated by Capacity_Lac. Reaction 5 describes the reversible entry of pyruvate into the mitochondrial TCA cycle. Reaction 6 describes the irreversible diversion of TCA flux towards CellComponents, inhibited by 2-DG at rate i2. Reaction 8 describes the irreversible entry of intracellular glutamine into the TCA cycle. Reaction 9 describes the irreversible consumption of mitochondrial O2 coupled to OxPP activity, inhibited by oligomycin at rate i1 and stimulated by FCCP at rate s1. Reaction 10 describes the uptake of extracellular*

oxygen (O2_ex) into the mitochondrial compartment, regulated by Capacity_O2. kf, forward rate constant; kr, reverse rate constant; i1, oligomycin inhibition rate; i2, 2-DG inhibition rate; s1, FCCP stimulation rate; 2-DG, 2-deoxy-D-glucose; FCCP, carbonyl cyanide 4-(trifluoromethoxy)phenylhydrazone; TCA, tricarboxylic acid cycle; OxPP, oxidative phosphorylation pathway.

The reactions in Figure 34 that regulate the functioning of the model. Reversible reactions are present at the level of conversion from glucose to pyruvate, from pyruvate to lactate, and from pyruvate to the entry into the Krebs cycle.[9,20].

4.6.2 Results of the model

In each of the following images, the data from experiment 5 can be seen inserted into SimBiology as a framework, on which the equilibrium constant values of the various equations were then modified so that the curves obtained from the model would overlap with the experimental data.

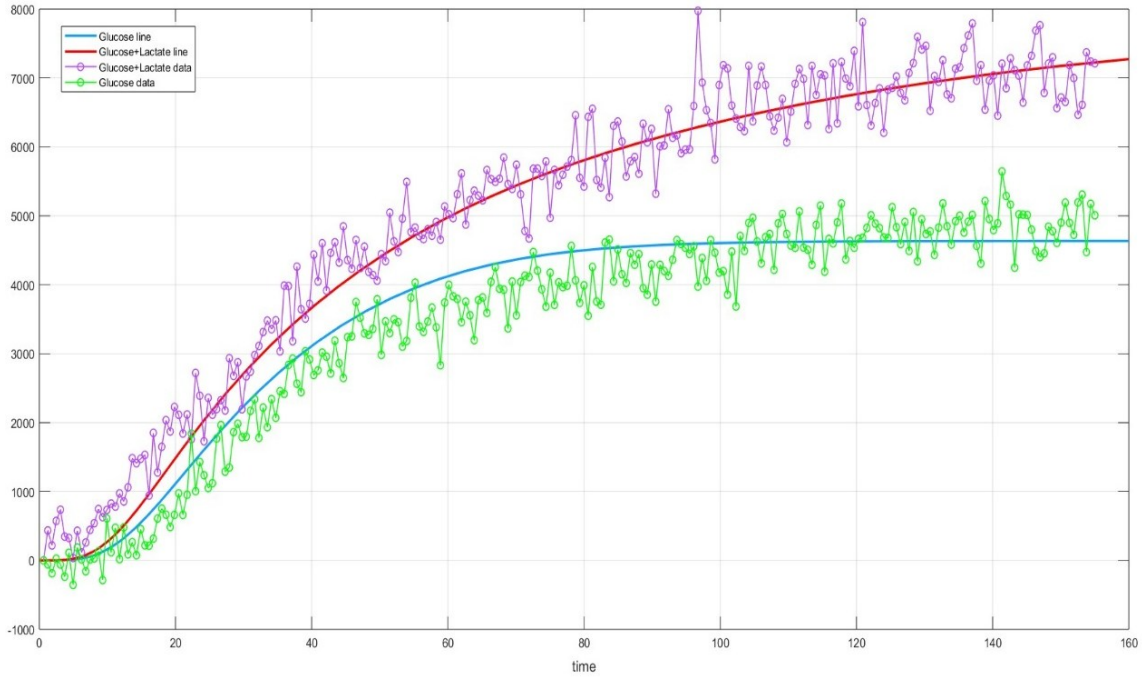

Figure 35 ***Model fitting of oxygen consumption kinetics in A549 cells under glucose and glucose + lactate conditions,*** *Simulated curves (lines) overlaid on experimental MitoXpress fluorescence data (circles) for A549 cells supplied with glucose alone (green circles) or glucose + lactate (purple circles). The model successfully reproduces the sigmoidal increase in oxygen consumption observed in both conditions, with glucose + lactate yielding a higher plateau fluorescence signal, consistent with lactate acting as an additional oxidative substrate entering the TCA cycle. Data are expressed as raw fluorescence (RFU). Time is expressed in minutes.*

In Figure 35 it can be seen how the fitting of the model lines with respect to those of glucose plus lactate and glucose plus glutamine are overlapping across all parts of the curves. It can therefore be understood how the addition of lactate to the medium led to an increase in O_2

consumption, motivated by the fact that lactate can be reintroduced into the cell as a substrate for the Krebs cycle, resulting in O_2 consumption as the final output.

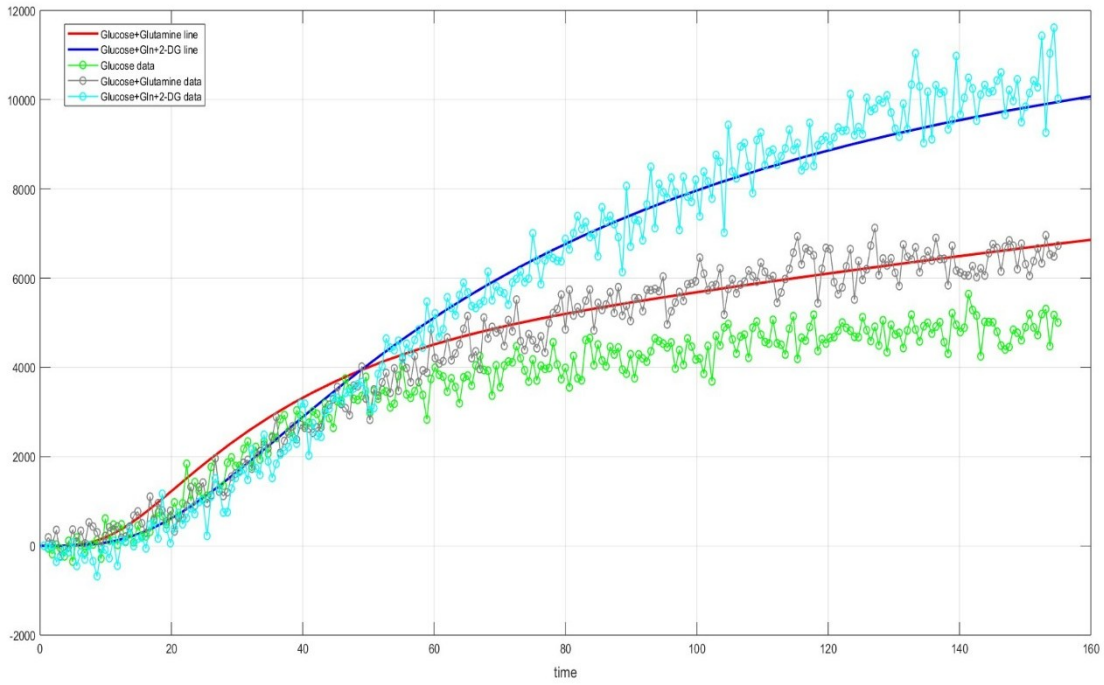

Figure 36 Model fitting of oxygen consumption kinetics in A549 cells under glucose + glutamine and glucose + glutamine + 2-DG conditions. Simulated curves (lines) overlaid on experimental MitoXpress fluorescence data (circles) for A549 cells supplied with glucose + glutamine (red line, grey circles) or glucose + glutamine + 2-DG (blue line, cyan circles). Glucose alone data (green circles) are shown as reference. Data are expressed as raw fluorescence (RFU). Time is expressed in minutes.

In Figure 36 it can be seen how O_2 consumption increases when using 2-DG, given that the cell is left with only the possibility of assimilating carbon substrates other than glucose, since that pathway is blocked; for this reason, glutamine is used directly as a substrate, entering the Krebs cycle, which concludes with oxidative phosphorylation, with a good equivalence between the obtained data and the model lines.

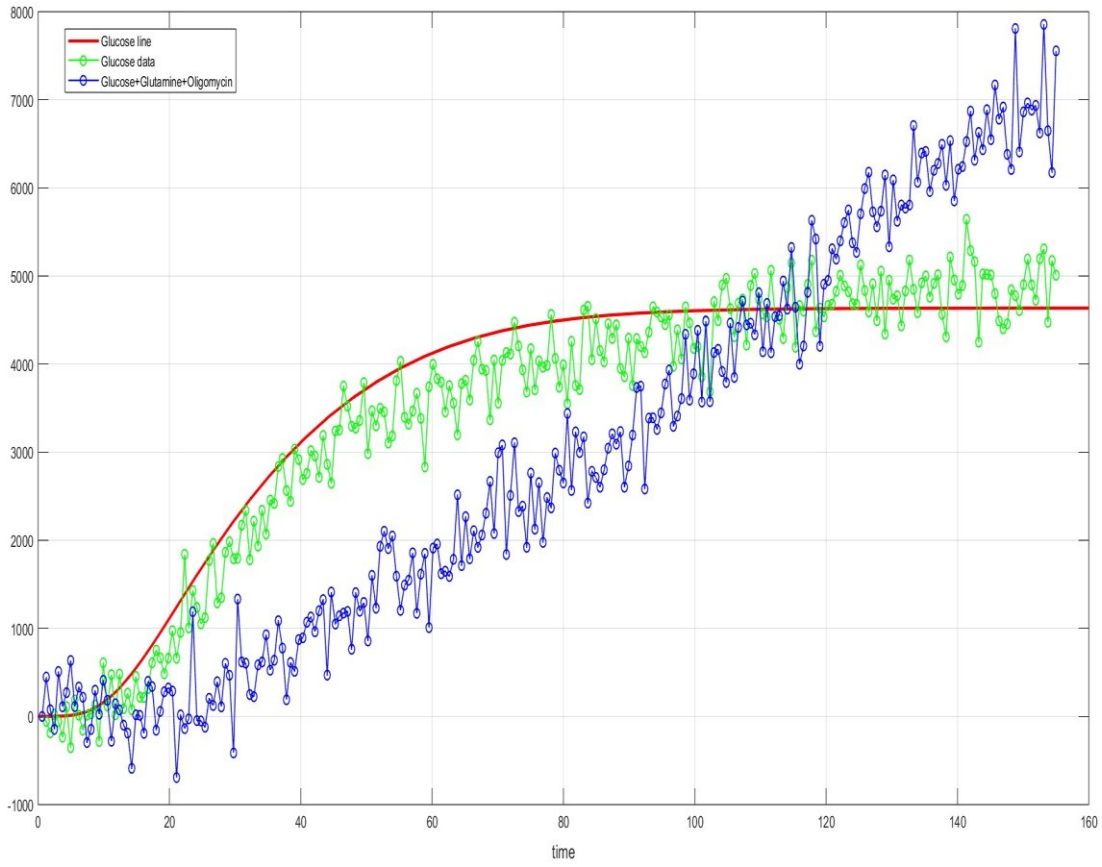

Figure 37 Simulated curve (red line) overlaid on experimental MitoXpress fluorescence data for A549 cells supplied with glucose alone (green circles), shown as reference alongside glucose + glutamine + oligomycin data (blue circles). Data are expressed as raw fluorescence (RFU). Time is expressed in minutes.

The construction of the oligomycin line in Figure 37 was very complex and no equilibrium constant values were found suitable for replicating the oligomycin trend; a higher level of programming would probably be needed to allow maximum customization of the effect that his compound has on oxidative phosphorylation.

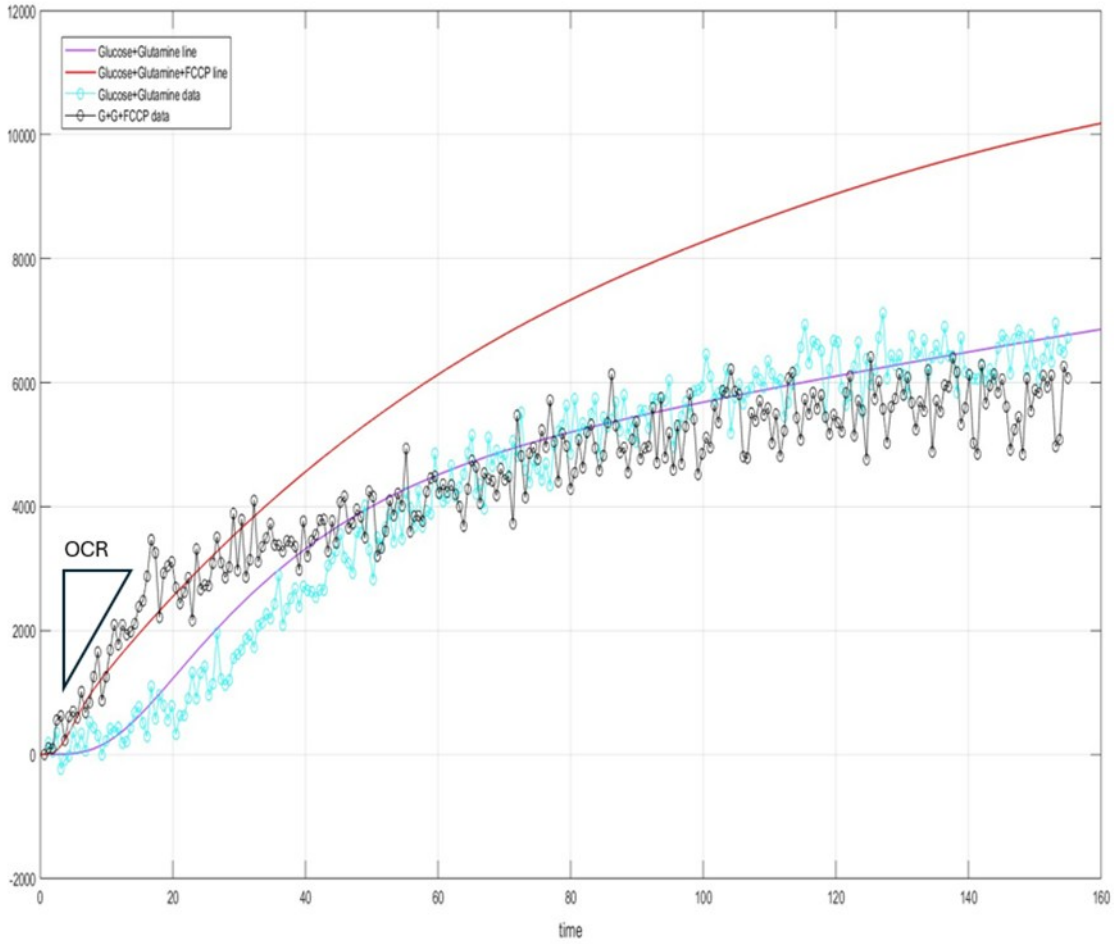

Figure 38 Simulated curves (lines) overlaid on experimental MitoXpress fluorescence data (circles) for A549 cells supplied with glucose + glutamine (purple line, cyan circles) or glucose + glutamine + FCCP (red line, black circles). The OCR, corresponding to the slope of the initial linear phase of the curve, is indicated by the dashed triangle. Data are expressed as raw fluorescence (RFU). Time is expressed in minutes.

The last construction can be seen in

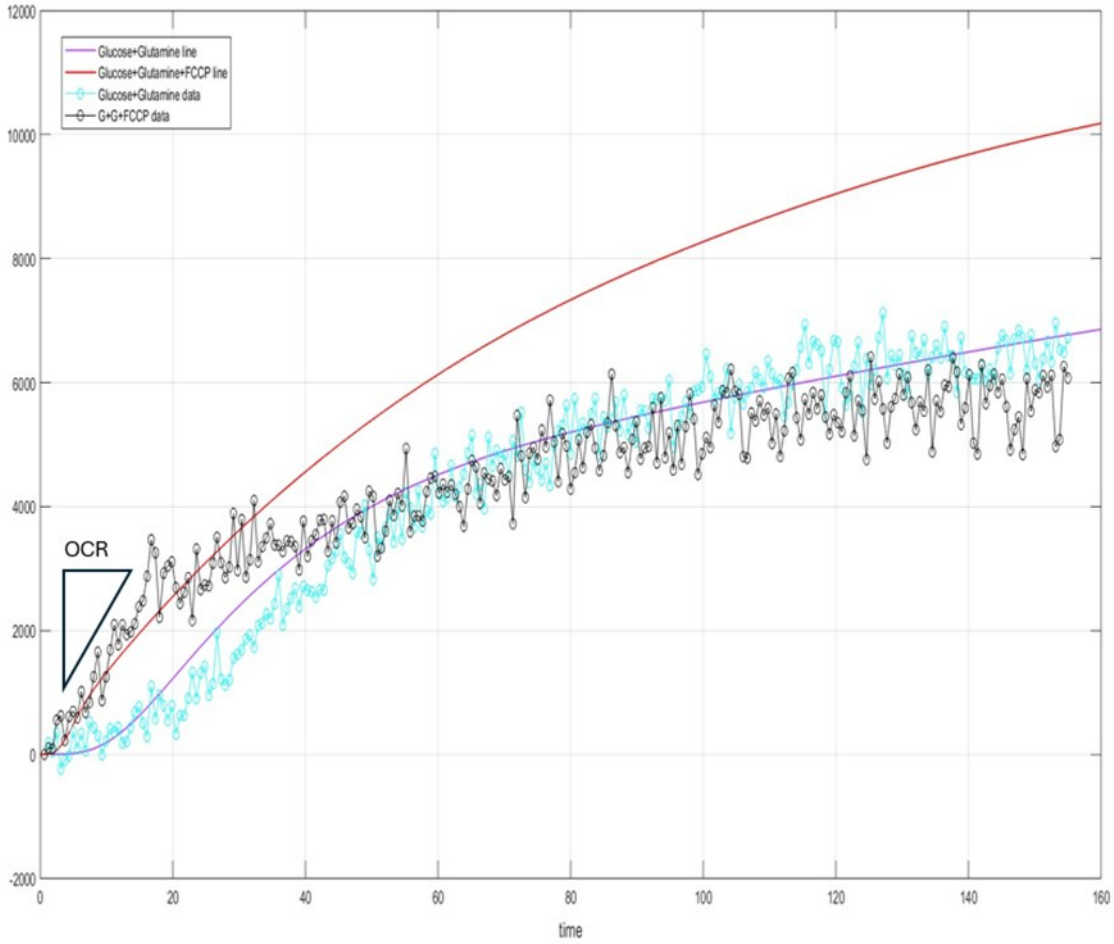

Figure 38; the model fitting for the glucose plus glutamine results manages to fit the line but regarding the FCCP line, the maximum that could be obtained is a slope of the curve (OCR) equal to the experimental one. Here as well, specific lines of code would probably be needed to build the model in a more tailored way for the cell line used.

5 CONCLUSIONS

The prediction of cell metabolism in certain diseases, such as cancer as addressed in this thesis, may seem like a utopia, yet it would allow targeted treatments and a potential reduction in side effects. It has been shown how the use of commercial methods for monitoring cell metabolism can highlight apparently simple behaviors that may provide important insights regarding the disease. This therefore leads to important conclusions about the actions to be taken and the path to follow in order to defeat a specific tumor. It has emerged how the metabolism of A549 cells is extremely active and much faster compared to the HepG2 cell line, which, even during the growth phase, showed considerable slowness and was therefore difficult to analyze; it probably has a much more functional glycolysis, as also highlighted by Nitin Patil and Zoreh Mirveis, and the Warburg effect must be very active[9,20]. The LLC-MK2 cell line also responded as expected by theory, being an immortalized cell line, particularly under starvation conditions. All cellular responses were consistent with the theoretical background presented at the beginning of this thesis. It has been observed how oligomycin manages to inhibit oxidative phosphorylation and is also used as an antibiotic, while 2-DG increases it by substituting glucose, thus increasing O_2 consumption. FCCP, as indicated by the manufacturer's manual, increased oxidative phosphorylation up to a bell-shaped plateau, as described by theory. At excessively high concentrations it could cause toxicity, as could oligomycin. By building the model, it has been observed how it is possible to replicate cell metabolism, albeit with some limitations, given that it was not possible to fully overlap the experimental lines with those constructed using the mathematical equations. Knowledge of numerical methods and MATLAB programming would be needed to create an ad hoc model and thus predict all metabolic steps. With further development and adequate programming knowledge, important insights could be obtained; it remains to be seen whether AI, the revolution of recent years, could bring mathematical model construction and scientific research to a higher level.

6 BIBLIOGRAPHY

(1) Bhat, G. R.; Sethi, I.; Sadida, H. Q.; Rah, B.; Mir, R.; Algehainy, N.; Albalawi, I. A.; Masoodi, T.; Subbaraj, G. K.; Jamal, F.; Singh, M.; Kumar, R.; Macha, M. A.; Uddin, S.; Akil, A. S. A.-S.; Haris, M.; Bhat, A. A. Cancer Cell Plasticity: From Cellular, Molecular, and Genetic Mechanisms to Tumor Heterogeneity and Drug Resistance. *Cancer Metastasis Rev* **2024**, *43* (1), 197–228. https://doi.org/10.1007/s10555-024-10172-z.

(2) Hanahan, D. Hallmarks of Cancer: New Dimensions. *Cancer Discovery* **2022**, *12* (1), 31–46. https://doi.org/10.1158/2159-8290.CD-21-1059.

(3) Ma, F.; Yu, W. The Roles of Lactate and Lactylation in Diseases Related to Mitochondrial Dysfunction.

(4) Mesquita, I.; Rodrigues, F. Cellular Metabolism at a Glance. In *Metabolic Interaction in Infection*; Silvestre, R., Torrado, E., Eds.; Experientia Supplementum; Springer International Publishing: Cham, 2018; Vol. 109, pp 3–27. https://doi.org/10.1007/978-3-319-74932-7_1.

(5) Zlacká, J.; Zeman, M. Glycolysis under Circadian Control. *IJMS* **2021**, *22* (24), 13666. https://doi.org/10.3390/ijms222413666.

(6) Vaupel, P.; Multhoff, G. Revisiting the Warburg Effect: Historical Dogma *versus* Current Understanding. *The Journal of Physiology* **2021**, *599* (6), 1745–1757. https://doi.org/10.1113/JP278810.

(7) Mulukutla, B. C.; Yongky, A.; Daoutidis, P.; Hu, W.-S. Bistability in Glycolysis Pathway as a Physiological Switch in Energy Metabolism. *PLoS ONE* **2014**, *9* (6), e98756. https://doi.org/10.1371/journal.pone.0098756.

(8) Arnold, P. K.; Finley, L. W. S. Regulation and Function of the Mammalian Tricarboxylic Acid Cycle. *Journal of Biological Chemistry* **2023**, *299* (2), 102838. https://doi.org/10.1016/j.jbc.2022.102838.

(9) Mirveis, Z.; Patil, N.; Byrne, H. J. Experimental and Computational Investigation of the Kinetic Evolution of the Glutaminolysis Pathway and Its Interplay with the Glycolysis Pathway. *FEBS Open Bio* **2024**, *14* (8), 1247–1263. https://doi.org/10.1002/2211-5463.13841.

(10) Kobayashi, A.; Takeiwa, T.; Ikeda, K.; Inoue, S. Roles of Noncoding RNAs in Regulation of Mitochondrial Electron Transport Chain and Oxidative Phosphorylation. *IJMS* **2023**, *24* (11), 9414. https://doi.org/10.3390/ijms24119414.

(11) Behl, T.; Makkar, R.; Anwer, Md. K.; Hassani, R.; Khuwaja, G.; Khalid, A.; Mohan, S.; Alhazmi, H. A.; Sachdeva, M.; Rachamalla, M. Mitochondrial Dysfunction: A Cellular and Molecular Hub in Pathology of Metabolic Diseases and Infection. *JCM* **2023**, *12* (8), 2882. https://doi.org/10.3390/jcm12082882.

(12) Pajak, B.; Siwiak, E.; Sołtyka, M.; Priebe, A.; Zieliński, R.; Fokt, I.; Ziemniak, M.; Jaśkiewicz, A.; Borowski, R.; Domoradzki, T.; Priebe, W. 2-Deoxy-d-Glucose and Its Analogs: From Diagnostic to Therapeutic Agents. *IJMS* **2019**, *21* (1), 234. https://doi.org/10.3390/ijms21010234.

(13) Xi, H.; Kurtoglu, M.; Liu, H.; Wangpaichitr, M.; You, M.; Liu, X.; Savaraj, N.; Lampidis, T. J. 2-Deoxy-d-Glucose Activates Autophagy via Endoplasmic Reticulum Stress Rather than ATP Depletion. *Cancer Chemother Pharmacol* **2011**, *67* (4), 899–910. https://doi.org/10.1007/s00280-010-1391-0.

(14) Mackieh, R.; Al-Bakkar, N.; Kfoury, M.; Roufayel, R.; Sabatier, J.-M.; Fajloun, Z. Inhibitors of ATP Synthase as New Antibacterial Candidates. *Antibiotics* **2023**, *12* (4), 650. https://doi.org/10.3390/antibiotics12040650.

(15) Hao, W.; Chang, C.-P. B.; Tsao, C.-C.; Xu, J. Oligomycin-Induced Bioenergetic Adaptation in Cancer Cells with Heterogeneous Bioenergetic Organization. *Journal of Biological Chemistry* **2010**, *285* (17), 12647–12654. https://doi.org/10.1074/jbc.M109.084194.

(16) Bertholet, A. M.; Natale, A. M.; Bisignano, P.; Suzuki, J.; Fedorenko, A.; Hamilton, J.; Brustovetsky, T.; Kazak, L.; Garrity, R.; Chouchani, E. T.; Brustovetsky, N.; Grabe, M.; Kirichok, Y. Mitochondrial Uncouplers Induce Proton Leak by Activating AAC and UCP1. *Nature* **2022**, *606* (7912), 180–187. https://doi.org/10.1038/s41586-022-04747-5.

(17) Toime, L. J.; Brand, M. D. Uncoupling Protein-3 Lowers Reactive Oxygen Species Production in Isolated Mitochondria. *Free Radical Biology and Medicine* **2010**, *49* (4), 606–611. https://doi.org/10.1016/j.freeradbiomed.2010.05.010.

(18) Strober, W. Trypan Blue Exclusion Test of Cell Viability. *CP in Immunology* **2015**,

111 (1). https://doi.org/10.1002/0471142735.ima03bs111.

(19) MitoXpress Xtra Oxygen Consumption Assay (HS Method).

(20) Patil, N.; Mirveis, Z.; Byrne, H. J. Kinetic Modelling of the Cellular Metabolic Responses Underpinning *in Vitro* Glycolysis Assays. *FEBS Open Bio* **2024**, *14* (3), 466–486. https://doi.org/10.1002/2211-5463.13765.

(21) Wu, C.-A.; Chao, Y.; Shiah, S.-G.; Lin, W.-W. Nutrient Deprivation Induces the Warburg Effect through ROS/AMPK-Dependent Activation of Pyruvate Dehydrogenase Kinase. *Biochimica et Biophysica Acta (BBA) - Molecular Cell Research* **2013**, *1833* (5), 1147–1156. https://doi.org/10.1016/j.bbamcr.2013.01.025.

(22) Gerencser, A. A.; Neilson, A.; Choi, S. W.; Edman, U.; Yadava, N.; Oh, R. J.; Ferrick, D. A.; Nicholls, D. G.; Brand, M. D. Quantitative Microplate-Based Respirometry with Correction for Oxygen Diffusion. *Anal. Chem.* **2009**, *81* (16), 6868–6878. https://doi.org/10.1021/ac900881z.

(23) Methods in Optical Oxygen Sensing: Protocols and Critical Analyses. In *Methods in Enzymology*; Elsevier, 2004; Vol. 381, pp 715–735. https://doi.org/10.1016/S0076-6879(04)81046-2.

(24) Orlicka-Płocka, M.; Gurda-Wozna, D.; Fedoruk-Wyszomirska, A.; Wyszko, E. Circumventing the Crabtree Effect: Forcing Oxidative Phosphorylation (OXPHOS) via Galactose Medium Increases Sensitivity of HepG2 Cells to the Purine Derivative Kinetin Riboside. *Apoptosis* **2020**, *25* (11–12), 835–852. https://doi.org/10.1007/s10495-020-01637-x.

(25) Xie, J.; Wu, H.; Dai, C.; Pan, Q.; Ding, Z.; Hu, D.; Ji, B.; Luo, Y.; Hu, X. Beyond Warburg Effect – Dual Metabolic Nature of Cancer Cells. *Sci Rep* **2014**, *4* (1), 4927. https://doi.org/10.1038/srep04927.

(26) Glycolysis Assay.